

# TECHNICAL SPECIFICATION



**Ultrasonics – Real-time pulse-echo scanners – Phantom with cylindrical, artificial cysts in tissue-mimicking material and method for evaluation and periodic testing of 3D-distributions of void-detectability ratio (VDR)**





## THIS PUBLICATION IS COPYRIGHT PROTECTED

Copyright © 2011 IEC, Geneva, Switzerland

All rights reserved. Unless otherwise specified, no part of this publication may be reproduced or utilized in any form or by any means, electronic or mechanical, including photocopying and microfilm, without permission in writing from either IEC or IEC's member National Committee in the country of the requester.

If you have any questions about IEC copyright or have an enquiry about obtaining additional rights to this publication, please contact the address below or your local IEC member National Committee for further information.

Droits de reproduction réservés. Sauf indication contraire, aucune partie de cette publication ne peut être reproduite ni utilisée sous quelque forme que ce soit et par aucun procédé, électronique ou mécanique, y compris la photocopie et les microfilms, sans l'accord écrit de la CEI ou du Comité national de la CEI du pays du demandeur.

Si vous avez des questions sur le copyright de la CEI ou si vous désirez obtenir des droits supplémentaires sur cette publication, utilisez les coordonnées ci-après ou contactez le Comité national de la CEI de votre pays de résidence.

IEC Central Office  
3, rue de Varembe  
CH-1211 Geneva 20  
Switzerland  
Email: [inmail@iec.ch](mailto:inmail@iec.ch)  
Web: [www.iec.ch](http://www.iec.ch)

### About IEC publications

The technical content of IEC publications is kept under constant review by the IEC. Please make sure that you have the latest edition, a corrigenda or an amendment might have been published.

- Catalogue of IEC publications: [www.iec.ch/searchpub](http://www.iec.ch/searchpub)

The IEC on-line Catalogue enables you to search by a variety of criteria (reference number, text, technical committee,...). It also gives information on projects, withdrawn and replaced publications.

- IEC Just Published: [www.iec.ch/online\\_news/justpub](http://www.iec.ch/online_news/justpub)

Stay up to date on all new IEC publications. Just Published details twice a month all new publications released. Available on-line and also by email.

- Electropedia: [www.electropedia.org](http://www.electropedia.org)

The world's leading online dictionary of electronic and electrical terms containing more than 20 000 terms and definitions in English and French, with equivalent terms in additional languages. Also known as the International Electrotechnical Vocabulary online.

- Customer Service Centre: [www.iec.ch/webstore/custserv](http://www.iec.ch/webstore/custserv)

If you wish to give us your feedback on this publication or need further assistance, please visit the Customer Service Centre FAQ or contact us:

Email: [csc@iec.ch](mailto:csc@iec.ch)  
Tel.: +41 22 919 02 11  
Fax: +41 22 919 03 00

# TECHNICAL SPECIFICATION



---

**Ultrasonics – Real-time pulse-echo scanners – Phantom with cylindrical, artificial cysts in tissue-mimicking material and method for evaluation and periodic testing of 3D-distributions of void-detectability ratio (VDR)**

INTERNATIONAL  
ELECTROTECHNICAL  
COMMISSION

PRICE CODE



---

ICS 17.140.50

ISBN 978-2-88912-377-3

## CONTENTS

FOREWORD.....	4
INTRODUCTION.....	6
1 Scope.....	7
2 Normative references .....	7
3 Terms and definitions .....	7
4 Symbols .....	11
5 Ambient conditions of measurement with the phantom.....	12
6 Specification of TMM 3D artificial anechoic-cyst phantom.....	12
6.1 3D-phantom concept .....	12
6.2 General phantom specification .....	12
6.3 TMM specifications:.....	12
6.4 Anechoic targets .....	13
6.5 Phantom enclosure.....	13
6.6 Scanning surface: .....	13
6.7 Dimensions .....	13
6.8 Phantom stability.....	14
6.9 Digitized image data.....	14
7 Principle of measurement using the 3D anechoic void phantom.....	15
7.1 General.....	15
7.2 Analysis .....	15
Annex A (informative) Description of construction of an example phantom and test results .....	17
Annex B (informative) System description.....	37
Annex C (informative) Rationale .....	38
Annex D (informative) Uniformity measurement .....	41
Bibliography.....	48
Figure A.1 – Example of measurement test equipment.....	17
Figure A.2a) – Package of TMM slices containing alternating void slices and attenuation slices of polyurethane foam .....	19
Figure A.2b) – Holes of different diameters in the void slices allow the use of the phantom with different ultrasound frequencies (1 – 15 MHz) .....	19
Figure A.2 – TMM slices .....	19
Figure A.3 – Structure of foam .....	19
Figure A.4 – C-images of voids .....	20
Figure A.5 – Experimental confirmation of Rayleigh distribution with attenuating TMM.....	21
Figure A.6 – Speed of sound in saltwater.....	22
Figure A.7 – Phantom with motor drive and two types of adapters .....	22
Figure A.8 – B-, D-, C- images and grey scale .....	24
Figure A.9 – Illustration of the VDR calculation for a ROI consisting of a single line.....	25
Figure A.10 – B-C-D planes .....	26
Figure A.11 – Principle of the ultrasound scanning array and beam .....	27
Figure A.12 – Schematic of B-D-C planes .....	28

Figure A.13 – 3D-Phantom images .....	29
Figure A.14 – B-D-C images and VDR .....	30
Figure A.15a) – Example: Curved Array, 40-mm radius, 3,5MHz with good VDR-values.....	31
Figure A.15b) – Example: Curved Array, 40-mm radius, 3,5MHz with poor VDR-values .....	31
Figure A.15 – VDR-values .....	31
Figure A.16 – Example: Linear array transducer 13 MHz.....	32
Figure A.17 – Interpretation of VDR parameter .....	33
Figure A.18 – Explanation of saturation (0-255 grey-scale range) .....	34
Figure A.19a) – Voids 2,5 mm.....	35
Figure A.19b) – Voids 3,0 mm.....	35
Figure A.19c) – Voids 4 ;0 mm.....	35
Figure A.19 – Saturation effect .....	35
Figure A.20 – Void spot analysis.....	35
Figure A.21a) – Local dynamic curve .....	36
Figure A.21b) – Expected envelope of VDR .....	36
Figure 21 – Local dynamic range .....	36
Figure C.1 – Autocorrelation function.....	39
Figure C.2a) – Autocorrelation function at 4,06 cm depth.....	40
Figure C.2b) – Autocorrelation function at 9,08 cm depth.....	40
Figure C.2 – Autocorrelation function – dependence on depth .....	40
Figure C.3 – Autocorrelation function at 10,94 cm depth.....	40
Figure D.1a) – Uniformity test with related linear or curved array transducer.....	42
Figure D.1b) – Fixed pattern in B-image .....	42
Figure D.1 – Uniformity test .....	42
Figure D.2a) – B-D-C image and fixed pattern in C-image.....	43
Figure D.2b) – Grey scale display of full array .....	43
Figure D.2 – Uniformity test – Additional features .....	43
Figure D.3 – Linear transducer with reference tape.....	44
Figure D.4 – Interpretation of simulated transducer failure when half of the probe is covered by five layers of 50-mm fabric tape .....	45
Figure D.5 – Disconnected elements, example with linear transducer .....	46
Figure D.6 – Example with curved array transducer and reference tape.....	47

## INTERNATIONAL ELECTROTECHNICAL COMMISSION

**ULTRASONICS – REAL-TIME PULSE-ECHO SCANNERS –  
PHANTOM WITH CYLINDRICAL, ARTIFICIAL CYSTS IN TISSUE-MIMICKING  
MATERIAL AND METHOD FOR EVALUATION AND PERIODIC TESTING  
OF 3D-DISTRIBUTIONS OF VOID-DETECTABILITY RATIO (VDR)**

## FOREWORD

- 1) The International Electrotechnical Commission (IEC) is a worldwide organization for standardization comprising all national electrotechnical committees (IEC National Committees). The object of IEC is to promote international co-operation on all questions concerning standardization in the electrical and electronic fields. To this end and in addition to other activities, IEC publishes International Standards, Technical Specifications, Technical Reports, Publicly Available Specifications (PAS) and Guides (hereafter referred to as “IEC Publication(s)”). Their preparation is entrusted to technical committees; any IEC National Committee interested in the subject dealt with may participate in this preparatory work. International, governmental and non-governmental organizations liaising with the IEC also participate in this preparation. IEC collaborates closely with the International Organization for Standardization (ISO) in accordance with conditions determined by agreement between the two organizations.
- 2) The formal decisions or agreements of IEC on technical matters express, as nearly as possible, an international consensus of opinion on the relevant subjects since each technical committee has representation from all interested IEC National Committees.
- 3) IEC Publications have the form of recommendations for international use and are accepted by IEC National Committees in that sense. While all reasonable efforts are made to ensure that the technical content of IEC Publications is accurate, IEC cannot be held responsible for the way in which they are used or for any misinterpretation by any end user.
- 4) In order to promote international uniformity, IEC National Committees undertake to apply IEC Publications transparently to the maximum extent possible in their national and regional publications. Any divergence between any IEC Publication and the corresponding national or regional publication shall be clearly indicated in the latter.
- 5) IEC itself does not provide any attestation of conformity. Independent certification bodies provide conformity assessment services and, in some areas, access to IEC marks of conformity. IEC is not responsible for any services carried out by independent certification bodies.
- 6) All users should ensure that they have the latest edition of this publication.
- 7) No liability shall attach to IEC or its directors, employees, servants or agents including individual experts and members of its technical committees and IEC National Committees for any personal injury, property damage or other damage of any nature whatsoever, whether direct or indirect, or for costs (including legal fees) and expenses arising out of the publication, use of, or reliance upon, this IEC Publication or any other IEC Publications.
- 8) Attention is drawn to the Normative references cited in this publication. Use of the referenced publications is indispensable for the correct application of this publication.
- 9) Attention is drawn to the possibility that some of the elements of this IEC Publication may be the subject of patent rights. IEC shall not be held responsible for identifying any or all such patent rights.

The main task of IEC technical committees is to prepare International Standards. In exceptional circumstances, a technical committee may propose the publication of a technical specification when

- the required support cannot be obtained for the publication of an International Standard, despite repeated efforts, or
- the subject is still under technical development or where, for any other reason, there is the future but no immediate possibility of an agreement on an International Standard.

Technical specifications are subject to review within three years of publication to decide whether they can be transformed into International Standards.

IEC 62558, which is a technical specification, has been prepared by IEC technical committee 87: Ultrasonics.

The text of this technical specification is based on the following documents:

Enquiry draft	Report on voting
87/434/DTS	87/458/RVC

Full information on the voting for the approval of this technical specification can be found in the report on voting indicated in the above table.

This publication has been drafted in accordance with the ISO/IEC Directives, Part 2.

The committee has decided that the contents of this publication will remain unchanged until the stability date indicated on the IEC web site under "<http://webstore.iec.ch>" in the data related to the specific publication. At this date, the publication will be

- transformed into an International standard,
- reconfirmed,
- withdrawn,
- replaced by a revised edition, or
- amended.

A bilingual version of this publication may be issued at a later date.

**IMPORTANT – The 'colour inside' logo on the cover page of this publication indicates that it contains colours which are considered to be useful for the correct understanding of its contents. Users should therefore print this document using a colour printer.**

## INTRODUCTION

This technical specification provides an example of a measurement method and of a test phantom. The specified method and test equipment permit operation without knowledge of proprietary information of the diagnostic ultrasonic equipment manufacturer.

This technical specification describes desirable specifications and performance characteristics of a tissue-mimicking material (TMM) 3D artificial-cyst phantom. An example including design of a realized and conforming phantom is given. The described results are independent of applied electronic and design architecture of diagnostic ultrasound systems and related transducers suitable for testing with the phantom.

Medical diagnostic ultrasound systems and related transducers need periodic testing as the quality of medical decisions based on ultrasonic images may decrease over time due to progressive degradation of essential systems characteristics. The TMM phantom is intended to be used to measure and to enable documentation of changes in void-detectability ratio in periodic tests over years of use.

The example of phantom design uses sliced TMM arranged as alternating "cyst-slices" and "attenuation-slices". It allows measurement along all three axes of the ultrasonic beam (axial, azimuthal and elevation) to determine the void-detectability ratio depending on the depth in the image generated from a transducer. The basis of the design concept and measurement method is anechoic, artificial cysts, representing idealized pancreatic ducts in the human body, and the measurement of the void-detectability ratio inside the images of these artificial cysts. The images of the artificial cysts should appear anechoic. The measurement of void-detectability ratio quantifies the diagnostic ultrasound system's ability to properly represent these objects. Increased artifactual signals appearing within images of these artificial cysts indicate a degradation of certain image parameters. A certain level of artifactual signals is to be expected for any ultrasound system, due to the emitted beam's shape and the transducer's receive characteristics. Any increase in these artifactual signals may be caused, for example, by grating- and side-lobes that may occur due to, for example, partial or total depolarisation of elements, delamination between transducer elements and lens, or corrosion. The measurement procedure allows a reliably and reproducibly determination of the visibility limits of small voids, an important image parameter of an ultrasound diagnostic system over the time of use, by applying dedicated acquisition, processing and documentation software.

Four informative annexes are provided: Annex A – Description of construction of an example phantom and test results; Annex B – System description; Annex C – Rationale; Annex D – Uniformity measurement.

# ULTRASONICS – REAL-TIME PULSE-ECHO SCANNERS – PHANTOM WITH CYLINDRICAL, ARTIFICIAL CYSTS IN TISSUE-MIMICKING MATERIAL AND METHOD FOR EVALUATION AND PERIODIC TESTING OF 3D-DISTRIBUTIONS OF VOID-DETECTABILITY RATIO (VDR)

## 1 Scope

This technical specification specifies essential characteristics of a phantom and method for the measurement of void-detectability ratio for medical ultrasound systems and related transducers. It is restricted to the aspect of long-term reproducibility of testing results.

This technical specification establishes:

- important characteristics and requirements for a TMM 3D artificial cyst phantom using anechoic voids;
- a design example of a 3D artificial cyst phantom, the necessary test equipment and use of relevant computer software algorithms.

This technical specification is currently applicable for linear array transducers. A uniformity test prior to void-detectability ratio (VDR) measurement is recommended.

NOTE The basic concept of the 3D artificial-cyst phantom may also be valid for other types of ultrasound transducers; however there is a need for further verification (see Annex D).

## 2 Normative references

The following referenced documents are indispensable for the application of this document. For dated references, only the edition cited applies. For undated references, the latest edition of the referenced document (including amendments) applies.

IEC 60050-802, *International Electrotechnical Vocabulary, Part 802: Ultrasonics*

## 3 Terms and definitions

For the purposes of this document, the terms and definitions contained in IEC 60050-802 as well as the following terms and definitions apply.

### 3.1

#### **acoustic coupling medium**

medium, usually fluid or a gel, that allows echo-free coupling of the transducer to the coupling window of the phantom.

### 3.2

#### **artifactual signal**

signal at a specific region in an image where no signal is expected (e.g. inside the image of a void)

### 3.3

#### **attenuation coefficient**

at a specified frequency, the fractional decrease in plane wave amplitude per unit path length in the medium, specified for one-way propagation

Units:  $\text{m}^{-1}$  (attenuation coefficient is expressed in dB  $\text{m}^{-1}$  by multiplying the fractional decrease by 8,686 dB)

[IEC 61391-2:2010, definition 3.4]

### 3.4

#### **backscatter coefficient**

at a specified frequency, the mean acoustic power scattered by a specified object in the  $180^\circ$  direction with respect to the direction of the incident beam, per unit solid angle per unit volume, divided by the incident beam intensity, the mean power being obtained from different spatial realizations of the scattering volume

Units:  $\text{m}^{-1}\text{steradian}^{-1}$

NOTE The frequency dependency should be addressed at places where backscatter coefficient is used, if frequency influences results significantly.

[IEC 61391-1:2006, definition 3.6, modified]

### 3.5

#### **backscatter contrast**

ratio between the backscatter coefficients of two objects or regions

[IEC 61391-2:2010, definition 3.8]

NOTE Backscatter contrast can be frequency-dependent but it is independent of any image system.

### 3.6

#### **B-, C-, D-image**

basic cross sectional presentations of 3D-images:

B-image is in a plane that is created by the acoustic scan-lines (scan plane);

C-image is in a plane perpendicular to the acoustic scan lines in the B-image;

D-image is in a plane perpendicular to B-image–plane and C-image-plane

### 3.7

#### **B-, C-, D-(image) plane**

B-plane: scan plane;

C-plane: reconstructed image plane that is perpendicular to acoustic scan lines in the B-plane;

D-plane: reconstructed image plane that is perpendicular to the scan plane and the C-plane

### 3.8

#### **coupling window**

portion of the phantom's enclosure provided for entrance and exit of the transmitted ultrasound waves to/from the tissue-mimicking material without significant attenuation or distortion

NOTE The coupling window usually consists of a thin membrane which protects the tissue-mimicking material from evaporation, leakage and mechanical damage by the transducer and which does not significantly alter the ultrasound signals

### 3.9

#### **detection limit**

smallest true value of the measurement, which is detectable by the measuring method

[IEC 60761-1:2002, definition 3.10, modified]

**3.10****digitized image data**

two-dimensional or three-dimensional set of pixel (voxel) values derived from the grey-level values of the B-mode images that are sent to the monitor screen

**3.11****documentation**

human-readable information about a device instance

[IEC 62453-1:2009, definition 3.1.18]

NOTE Within the context of this TS, the printed documentation and the documentation provided via Extended Markup Language (XML) are also meant. The documentation can consist of several documents and images.

**3.12****fixed pattern**

parts of the B-mode image that remain in the same position relative to the image frame when the transducer is moved

**3.13****grey-level value**

number determining the brightness of the pixels of a B-mode image (as derived from the signal amplitude of the signal reflected from the corresponding position in the body)

NOTE The grey level values determine the brightness of specific pixels in the image and they historically range from 0 (black) to 255 (white). Black indicates a weak signal, white a strong signal. This convention holds throughout this document for calculations. In images an inverted display can be used, where black indicates the level 256 and white 0.

**3.14****(acoustic) scan line**

one of the component lines that form a B-mode image on an ultrasound system monitor, where each line is the envelope-detected A-scan line in which the echo amplitudes are converted to brightness values

[IEC 61391-1:2006, definition 3.26, modified]

**3.15****scan plane**

acquired image plane containing the acoustic scan lines

[IEC 61391-2:2010, definition 3.30]

**3.16****specific attenuation coefficient**

at a specified frequency, the slope of attenuation coefficient plotted against frequency

Units:  $\text{m}^{-1} \text{Hz}^{-1}$

**3.17****Tissue-mimicking material****TMM**

material in which the propagation velocity (speed of sound), reflection, scattering, and attenuation properties are similar to those of soft tissue for ultrasound in the frequency range 1 MHz to 15 MHz

[IEC 61391-1:2006, 3.36, modified]

### 3.18

#### **TMM 3D artificial anechoic cyst phantom**

phantom containing tissue-mimicking material, in which there are well-defined regions whose backscatter contrast is lower than -60 dB relative to the regions containing TMM

### 3.19

#### **uniformity test procedure**

procedure to test the uniformity of the transmitted signals of all the elements of array transducers

### 3.20

#### **void**

artificial anechoic cyst

region of defined geometry in a tissue-mimicking material that generates no scattered acoustic waves

NOTE Saline solution in specified concentration is known to produce extremely low levels of scattered signals and therefore it is an optimal approximation to a perfect void.

### 3.21

#### **void-detectability ratio**

##### **VDR**

number characterizing the visibility of an image area corresponding to a void of defined diameter surrounded by tissue-mimicking material (TMM) in the phantom

$$VDR = (\mu_1 - \mu_2) / \sigma_1 = (1/n)(\sum_{i=1..n}(VDR_i))$$

where

$\mu_1$  = mean image pixel value of the TMM in the region surrounding the void for a given C-plane;

$\mu_2$  = mean value of the image pixel values from within the image area representing a void;

$\sigma_1$  = standard deviation of mean pixel values over separate TMM areas equal to the void area and lying in the region of the void, for a given C-plane;

$n$  = number of voxels (pixels) from a given C-plane or from a specific part of this C-plane (e.g. the image area of a single void or the image area of all voids within the C-plane)

NOTE 1 The image of the surrounding TMM material is expected to show modulated grey levels (i.e. an ultrasound speckle image) due to the ultrasound interference patterns).

NOTE 2: The VDR formula is derived from [4]<sup>1</sup>

#### **3.21.1**

##### **detectability ratio for a single voxel**

detectability ratio for a single voxel is defined by:

$$VDR_i = (\mu_1 - g_i) / \sigma_1$$

where

$\mu_1$  = mean image pixel value of the TMM in the region surrounding the void for a given C-plane;

$g_i$  = grey level value of the i-th voxel (pixel) from a given C-plane or from a specific part of this C-plane (e.g. the image area of a single void or the image area of all voids within the C-plane);

$\sigma_1$  = standard deviation of mean pixel values over separate TMM areas equal to the void area and lying in the region of the void, for a given C-plane

<sup>1</sup> Numbers in square brackets refer to the Bibliography.

NOTE The VDR formula is derived from [4].

### 3.21.2

#### maximum VDR within a void

$VDR_V$

maximum VDR within a void is defined by

$$VDR_V = (\mu_1 - g_V) / \sigma_1 = \max_{i=1..n} (VDR_i)$$

where

$\mu_1$  = mean image pixel value of the TMM in the region surrounding the void for a given C-plane;

$g_V$  = minimum grey-level value of the image region corresponding to the interior of a void;

$\sigma_1$  = standard deviation of mean pixel values over separate TMM areas equal to the void area and lying in the region of the void, for a given C-plane

NOTE The VDR formula is derived from [4].

#### maximum VDR in a ROI in a C-plane

$VDR(max)$

maximum value of VDR in a specified region of interest (ROI) within a C-plane

### 3.21.3

#### absolute maximum VDR in a ROI in a volume

$VDR_{absmax}$

absolute maximum value of all  $VDR_i$ -values in a volume comprising the evaluated region of interest (ROI), i.e. in a display of the function  $VDR(max)$  over the total depth  $z$  in the evaluated ROI

### 3.22

#### VDR limit

minimum value of the VDR for which there is visualization of a void on an ultrasound image

NOTE In [4] the detection limit for the detection of voids of the defined void sizes (see A.10.1) for a noise level independent of electronic noise was stated to be around  $VDR = 2,5$  for spherical voids.

## 4 Symbols

$c$  = speed of sound

$g_{i..}$  = grey level value of the  $i$ -th voxel (pixel) from a given C-plane or from a specific part of this C-plane (e.g. the image area of a single void or the image area of all voids within the C-plane)

$g_V$  = minimum grey-level value of image region corresponding to the interior of a void

$T$  = temperature

$S$  = salinity

$S_{g \max}$  = maximum value of the digitized image data (grey-level values)

$VDR$  = void detectability ratio -- averaged value over the image of a void

$VDR_i$  = detectability ratio for a single voxel (pixel)  $i$ , measured over a region in the digitized image data

$VDR_V$  = void detectability ratio -- maximum value within the image of a void

$VDR(max)$  = maximum value of VDR in a specified ROI in a C-plane

$VDR_{absmax}$  = absolute maximum value of VDR in a display of the functional range of  $VDR(max)$  over depth

$z$	=	depth
$\mu_1$	=	mean image pixel value of the TMM in the region surrounding the void for a given C-plane
$\mu_2$	=	mean value of the image pixel values from within the image area representing a void
$\mu_3$	=	mean value of the image pixel values from a 3D region of interest (ROI)
$\sigma_1$	=	standard deviation of mean pixel values over separate TMM areas equal to the void area and lying in the region of the void, for a given C-plane

## 5 Ambient conditions of measurement with the phantom

Typical ambient conditions during measurements should be similar to those specified in IEC 61319-1 and IEC 61319-2:

Temperature: 20 °C to 24 °C;

Relative humidity: 45 % to 75 %;

Atmospheric pressure: 86 kPa to 106 kPa.

## 6 Specification of TMM 3D artificial anechoic-cyst phantom

### 6.1 3D-phantom concept

The 3D phantom shall be composed of TMM that contains an arrangement of voids of a specified shape (i.e. cylindrical) and sizes specified in relation to the defined frequency range of transducers to be tested.

NOTE An example of a phantom that conforms to this technical specification is presented in Annex A.

### 6.2 General phantom specification

The phantom shall allow implementing the test procedures described in this document by providing anechoic targets at known locations within tissue-mimicking material. Analysis of images is done from digitized image data that are acquired during scans of the phantom. The manufacturer shall provide an instruction manual with advice regarding reliable use and maintenance.

### 6.3 TMM specifications:

The following parameters of the TMM shall lie within the specified limits:

**Speed of sound:**  $(1\,540 \pm 10)$  m s<sup>-1</sup> at 3 MHz

**Density:**  $(1,00 \pm 0,11)$  g cm<sup>-3</sup>

**Specific attenuation coefficient:**  $(0,7 + 0,2 / - 0,05)$  dB cm<sup>-1</sup>MHz<sup>-1</sup> in the 1 MHz to 15 MHz range. If a phantom is manufactured by using layered materials as in Annex A, for example, the specific attenuation coefficient corresponding to the mean value of the specific attenuation shall apply.

**Backscatter coefficient:**  $(3 \times 10^{-4} \text{ cm}^{-1}\text{sr}^{-1}) \pm 10$  dB at 3 MHz; with a “frequency to the  $n$ ” ( $f^n$ ) dependence, where  $2 < n < 4$  from 1 MHz to 15 MHz. The value of the backscatter coefficient of the phantom shall be reported as a function of frequency, together with the results obtained with the phantom. Scatterers within the phantom should be of a sufficient number density to provide Rayleigh statistics in the echo-amplitude distribution (see Figure A.2.2). The scatterer number density needed will depend on the frequency and focusing characteristics of the transducer and ultrasound system to be tested under this technical

specification. For guidance, around 10 scatterers per cubic millimetre are sufficient for most transducers operating up to 15 MHz.

Phantoms manufactured to these TMM specifications can be constructed using, for example, open pore sponges or polyurethane foam immersed in saline. The materials have microscopic inhomogeneities that are uniformly distributed throughout to produce the desired attenuation level.

#### **6.4 Anechoic targets**

Anechoic targets shall be provided whose backscatter contrast is at least -60 dB relative to that of the background TMM material. Degassed saline solution is an adequate material for filling anechoic targets. The saline shall be adapted in concentration to achieve sound speed of  $(1\,540 \pm 10) \text{ m s}^{-1}$ . The sound speeds in saltwater as a function of saline concentration and temperature is shown Figure A.2.3.

Anechoic targets shall be placed at different depths throughout the phantom volume. Targets of a given diameter shall be positioned with their centres coplanar, so that in the scan plane at least 6 such targets are viewed at different lateral locations at each depth from the transducer. Targets shall be positioned in lateral locations so that they can be viewed from different locations within the scanning plane. Targets in the phantom presented in Annex A are cylinders whose faces are parallel to the scanning surface.

At each depth and lateral location, various sizes of anechoic targets shall be available. For each frequency region two sizes of voids shall be present. Dimensions of voids shall be selected in regard to realistic azimuthal and elevational beam width and frequency of the transducer, as follows:

- Voids of 4 mm and 2,5 mm diameter are satisfactory for transducers operating in the 1 MHz to 4 MHz range.
- Voids of 3 mm and 1,5 mm diameter are satisfactory for transducers operating in the 4 MHz to 8 MHz range
- Voids of 2,5 mm and 1 mm diameter are satisfactory for transducers operating in the 8 MHz to 15 MHz range

One important reason for the occurrence of artifactual signals inside of anechoic voids are side-lobes of the ultrasonic beam [9], A prerequisite to detect artifactual signals caused by side-lobes and/or grating-lobes in images of anechoic voids is an echo-amplitude difference better than -60 dB compared to the surrounding tissue-mimicking material.

#### **6.5 Phantom enclosure**

The purpose of this enclosure is to protect the contents from degradation (fluid evaporation) with time during use and storage. The material used for the enclosure walls shall be such as to prevent degradation of the contents.

#### **6.6 Scanning surface**

The scanning surface shall allow acoustic contact of the entire active surface of the transducer with the phantom. If the scanning surface includes a window material, such as a foil or membrane, to prevent desiccation of the TMM or to protect the TMM contents from damage from the transducer, the membrane properties, including material contained therein, thickness, density, and specific attenuation coefficient, shall be provided. Alternatively, transmission losses as a function of frequency shall be provided.

#### **6.7 Dimensions**

The dimensions of the phantom shall be suitable to evaluate transducers by assessing VDR at least 2/3 of the imaged field for which the transducer is typically used. For example, a

ultrasound system that provides a 24 cm imaging depth requires a phantom of at least 16 cm depth. This is generally at least four times the size of the transducer transmit-receive aperture, so any degradation caused by side lobes or by poor lateral resolution would be manifested within this range.

### 6.8 Phantom stability

The manufacturer shall state the duration of stability and indicate criterion of use.

### 6.9 Digitized image data

Test and analysis methods described in this technical specification are applied to digitized image data derived from the ultrasound system and related transducer being evaluated. In all cases, grey level values for all spatial locations in the image must be available. Image data typically are in a matrix consisting of about  $300 \times 300$  pixels and at least 8 bits (256 levels) of amplitude (directly proportional to grey-scale) resolution.

Digitized image data may be obtained using a video frame grabber to digitize images from output connectors normally used to transfer images to analogue monitors or to recording devices. The video signal digitization must be provided under exactly specified conditions to avoid or minimize signal distortions. Specific care and attention shall be taken for the following parameters:

- The input dynamic range of the video-frame grabber shall be adjusted according to the maximum signal amplitude of the video output.
- The digitizing amplitude resolution (given by the pixel byte size) shall be better than that of the grey-scale resolution of the ultrasound image video-output signal. A minimum of 8 bits or 256 grey levels is required.
- Ultrasound image signal to TV conversion-function linearity has to be assured. The spatial resolution (given by the voxel size) of the digital picture must be better than the original video line density of the image.
- The video-capture frame rate of the video-frame grabber must be high enough to allow acquisition of data to keep up with input data rates, if the imaged field is moved. Keep in mind the difference between scanning frame rate and output video frame rate.
- A cable matched for input/output impedance has to be used to avoid reflections in the line. A cable length of 1 m to 2 m is generally not critical.
- The digitized image data must be representative of those on the display monitor of the diagnostic ultrasound system. The digitized image data derived from the diagnostic ultrasound system shall not undergo any post-processing modifications between the point of data processing and the monitor output signal of the system before being subjected to analysis as described in this technical specification.

Data also can be acquired using DICOM-images (Digital Imaging and Communications in Medicine) [13] or images in other formats from the ultrasound system. This method is used by most ultrasound system manufacturers for in-house quality-control testing and image-processing development. Capabilities often exist to extend the method for use by clinical personnel using, for example, file-transfer-protocol (ftp) resources.

Alternatively, many diagnostic ultrasound systems provide image files on removable media, such as USB-thumb drives, magneto-optical disks, zip disks, or CD-ROM, and these are appropriate sources of digital images data as well.

In addition, many imaging centres use commercially available Picture Archiving and Communication Systems (PACS) for viewing and storing ultrasound-image data. Manufacturers of PACS systems usually provide means to acquire images in an uncompressed format, such as a tiff (Tagged Image File Format) or a DICOM format, to workstations that have access rights to the image data.

In any case, where image data are not acquired from the (analogue or digital) video output but from data derived within the ultrasound system, it must be ascertained that the digitized amplitude provided in this case really corresponds to the grey-levels shown on the viewing screen.

Until DICOM offers a standard for 3D-images the best procedure is to use a VGA or DVI converter to digitize the video output signal of the ultrasound system.

## 7 Principle of measurement using the 3D anechoic void phantom

### 7.1 General

The measurement equipment for the VDR measurement consists of the phantom, the transducer and ultrasound system to be tested, and a means to acquire digitized image data from scan planes that extend over that volume of the phantom that contains voids.

An acceptable method for acquiring the 3D data is to apply the mechanical transducer positioner described in Annex A, then to record digitized image data from closely positioned scan planes. The scan plane spacing should be equal to the voxel separation within the scan-planes, however; it should be less than 1/4 times the diameter of the void from which VDR will be computed.

Other approaches to 3D data acquisition are to use special transducers, such as those with built-in mechanical translation of the probe, or to use manual translation of the transducer while recording image data in a cine image loop, such as those provided within the ultrasound system. However, the latter approach does not allow for ensuring an appropriate B-plane spacing.

A uniformity measurement of transducers is essential. It should be done prior to VDR measurement. One possible method is described in Annex D.

### 7.2 Analysis

The following is an acceptable method of analysis:

VDR is computed for anechoic targets (i.e., voids) of a given diameter, depth, and lateral location in planes parallel to accessible C-planes, as described in Annex A. However, for this technical specification, results shall be reported for C-planes containing voids.

Within images reconstructed from the acquired 3D data a region of interest (ROI) is defined.

The data in this region shall provide cubic voxels (i.e. the dimensions of the voxel should be identical in all three directions) of known size. To achieve this objective, information on the image scale must be acquired. The 3D-ROI data are stored in a matrix to allow viewing and processing of this 3D-data set.

For each C-plane within the 3D-ROI the mean ( $\mu_1$ ) and the standard deviation ( $\sigma_1$ ) values for the TMM are calculated. Different approaches for excluding void regions from these calculations have been proposed. Some of these approaches make use of the additional information from the knowledge of the void distribution; others just use the local grey-scale compared to the other voxel amplitudes within the C-plane to decide whether or not the individual voxel is part of a void. Different approaches to exclude void regions from the calculation of the TMM-mean and standard deviation are described in Annex A.

The  $\mu_1$  and  $\sigma_1$  values are used to calculate  $VDR_i$  for each individual voxel according to the expression

$$VDR_i = (\mu_1 - g_i) / \sigma_1 \quad (1)$$

giving a 3D-data set.

The  $VDR_i$  values are stored in a matrix similar to the matrix containing the 3D-ROI grey-scale information-set to allow direct viewing and further processing.

The  $VDR_i$  values are evaluated for each C-plane. There are different approaches to this evaluation. Either statistical data can be derived directly for a complete C-plane or the VDR-data can be first calculated for each void and then the information of the individual voids can be subsumed in one information-set for the plane. Statistical evaluation can use calculation of either mean values of VDR or maximum values of VDR.

NOTE 1 Maximum values are a reasonable approach, as the grey-scale distribution within each void shows a sharp drop towards the centre of the void (see Annex A) and experience shows that visibility of the void is strongly correlated to this maximum value.

Mean values are more difficult to obtain, as the border for each void must be defined, either by defining an amplitude limit or by using additional information on the location of the individual void.

NOTE 2 This determination of the void edges is the main source of error for the mean evaluation.

The mean or the maximum VDR-values of all the C-planes are plotted in a graph giving VDR over depth. Statistics may be performed on these data by offering a fitted curve.

A void of a given diameter and location shall be called detectable if its value of VDR exceeds 2,5. The range where the VDR-plot exceeds this value is the useful working range for the void diameters contained in this ROI [4].

The stored ROI grey-scale and the  $VDR_i$  3D-data sets are used to visually check the automated evaluation of the transducer.  $VDR_i$  visualisation of non-void regions is also important, as it reveals where the interference-pattern will give the impression of voids where there are none.

NOTE 3 The  $VDR_i$ -values on their own do not represent relevant information, but in the context of all the other  $VDR_i$ -values within an image of a void, a C-plane or a ROI, they are fundamental values for obtaining a 3D-image of the VDR-levels, mean values of VDR inside an image of a single void or a group of voids and maximum values of VDR in an image of a single void or a group of voids.

## Annex A (informative)

### Description of construction of an example phantom and test results

#### A.1 General

In this annex the construction and properties of a particular phantom satisfying the technical specification are described, together with examples of tests performed with it.

The equipment required for the VDR measurement consists of a phantom, transducer positioning slider with platform, PC (or Notebook) including software for image recording and analysis and hardware for making connections to the video output of the diagnostic ultrasound system and the positioning slider (see Figure A.1).

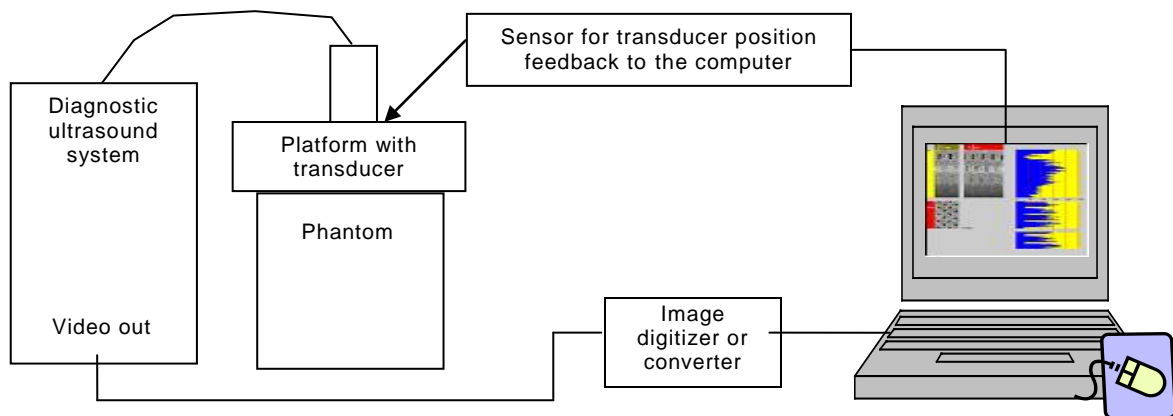


**Figure A.1 – Example of measurement test equipment**

This arrangement is suitable for testing linear array transducers as well curved arrays under certain conditions (see Annex D).

#### A.1.1 Definitions applicable to Annex A

##### A.1.1.1

##### **data acquisition system**

centralized system receiving data from one or more remote points

NOTE 1 Data may be transported in either analog or digital form and digitised thereafter if necessary.

NOTE 2 In the present case data are acquired via a frame grabber or converter from the available output signals of a diagnostic ultrasound system.

[IEC 62270:2004, 3.14]

##### A.1.1.2

##### **slice**

layer of attenuating and backscattering TMM

**A.1.1.2.1****attenuation slice**

layer of TMM having an attenuation coefficient greater than the average attenuation coefficient of an assembled phantom

**A.1.1.2.2****void slice**

layer of TMM containing voids and having an attenuation coefficient less than the average attenuation coefficient of an assembled phantom

**A.1.1.3****TCC<sup>2)</sup>-3D artificial anechoic cyst phantom**

phantom containing defined, alternating, attenuation- and void slices of backscattering material, oriented mainly perpendicular to the direction of sound propagation, and filled with an anechoic liquid material, such that the speed of sound and the mean attenuation and backscatter coefficients of the phantom closely approximate those of human soft tissue

**A.2 Phantom****A.2.1 General**

The example phantom is housed in a tight plastic box with external dimensions: height 22 cm × length 15 cm × width 8 cm.

The body of the phantom consists of alternating layers of polyurethane foam (attenuation slices and void slices), each with a thickness of 5 mm. Every second layer (the void slices) contains artificial cylindrical voids, which are cut into the foam (see Figures A.2, A.3 and A.4). Foam and voids are soaked with degassed 7 % (by weight) saline water. The concentration of the saline is adjusted so that the speed of sound of the soaked foam is  $1\,540 \pm 10 \text{ m s}^{-1}$  at 20 °C. It was found that the backscattering level for both foams immersed in saline was the same.

NOTE Polyurethane foam as recommended is available from different manufacturers worldwide. The material is very stable.

The packet of slices has a height of approximately 18 cm. After filling the phantom with saline, evacuation is necessary to remove retained air bubbles. The phantom is completely sealed with a 0,25 mm polyurethane foil over the first void slice. The foil is used as a coupling window with area  $11 \times 5,5 \text{ cm}^2$ ; it has a negligible attenuation.

---

2) Tissue Characterization Consulting, A-4850 Timelkam Austria. This information is given for the convenience of users of this document and does not constitute an endorsement by IEC of the company cited.

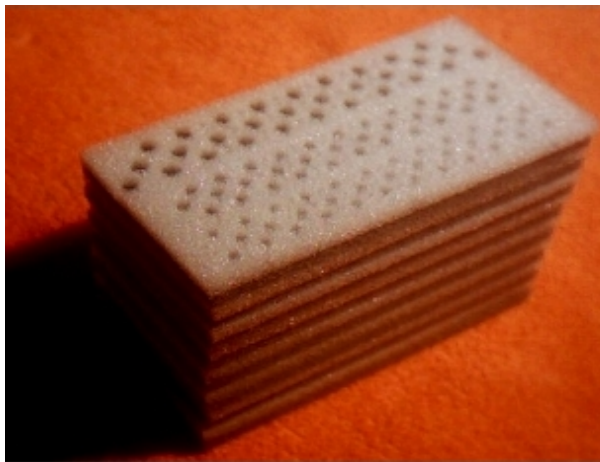


**Figure A.2a) – Package of TMM slices containing alternating void slices and attenuation slices of polyurethane foam**

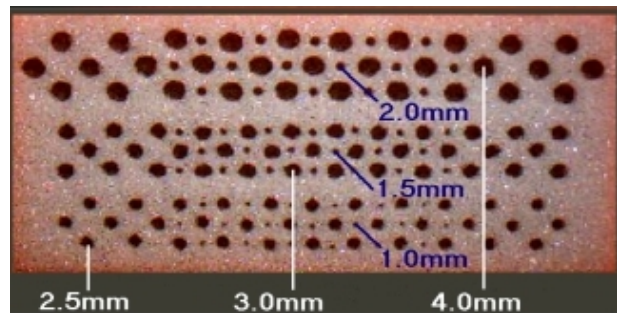


**Figure A.2b) – Holes of different diameters in the void slices allow the use of the phantom with different ultrasound frequencies (1 – 15 MHz)**

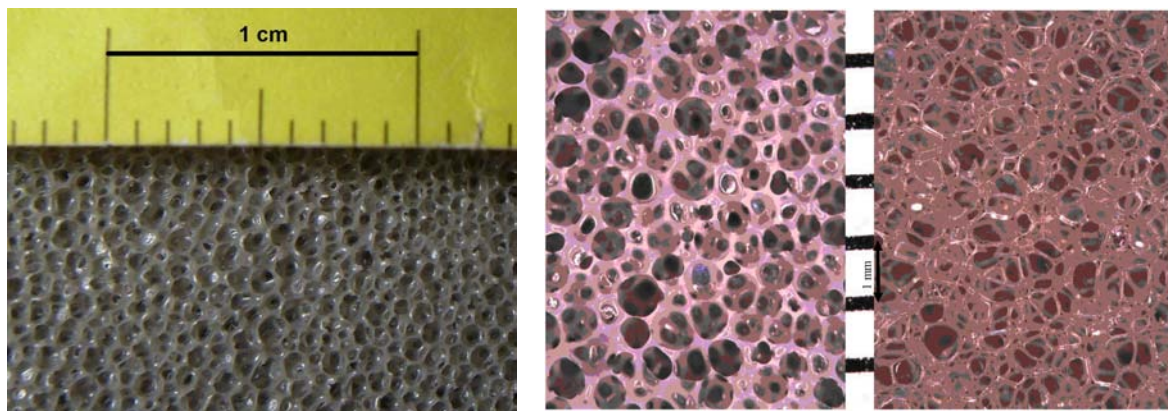
**Figure A.2 – TMM slices**

The foam of the attenuation slices has a density of  $120 \text{ kg m}^{-3}$  to  $130 \text{ kg m}^{-3}$ ; in the void slices it is  $20 \text{ kg m}^{-3}$  to  $30 \text{ kg m}^{-3}$ . The foam has attenuating and back-scattering properties. For the attenuation slices, the specific attenuation coefficient it is about  $0,7 \text{ dB cm}^{-1} \text{ MHz}^{-1}$ ; for the void slices it is about  $0,2 \text{ dB cm}^{-1} \text{ MHz}^{-1}$ . Thus, the mean specific attenuation coefficient of the phantom is about  $0,45 \text{ dB cm}^{-1} \text{ MHz}^{-1}$ .

The attenuation slices are used to attenuate the ultrasound pulses because the “void slices” do not attenuate them. In this way signal enhancement by artificial cysts is avoided. By having the voids with their low attenuation coefficient embedded within layers of the phantom that themselves have a low attenuation coefficient, distal enhancement artefacts caused by voids are negligible.

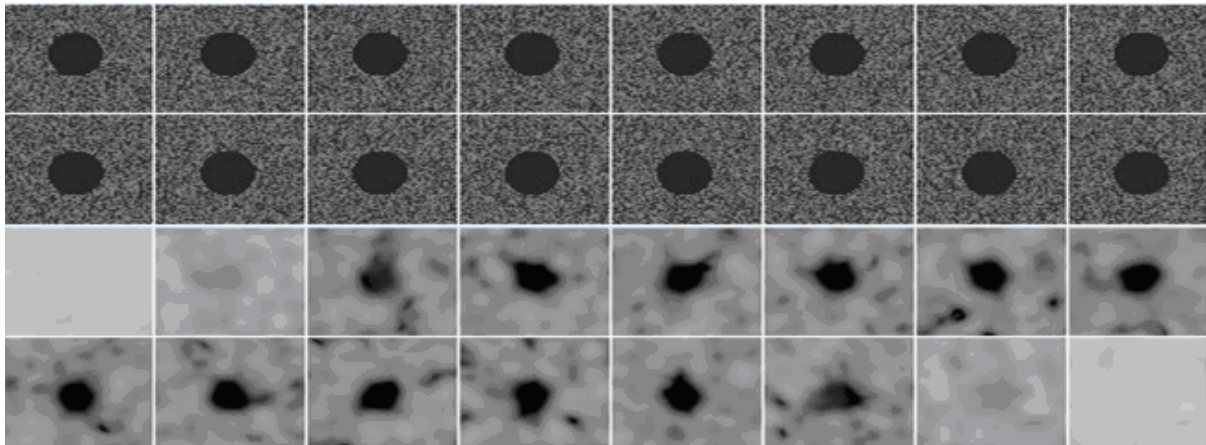
### A.2.2 Structure of foams

The foams have open pore walls; the thickness of the walls of the pores are in the range  $0,1 \text{ mm}$  to  $0,25 \text{ mm}$  (See Figure A.3). It is important that this size is not larger than the wavelength of the investigated ultrasound in order to obtain scattering.



Left: Cross section through the foam. Middle: Enlarged view, of the foam of the attenuation-slices. Right: Enlarged view of foam of the void-slices.

**Figure A.3 – Structure of foam**



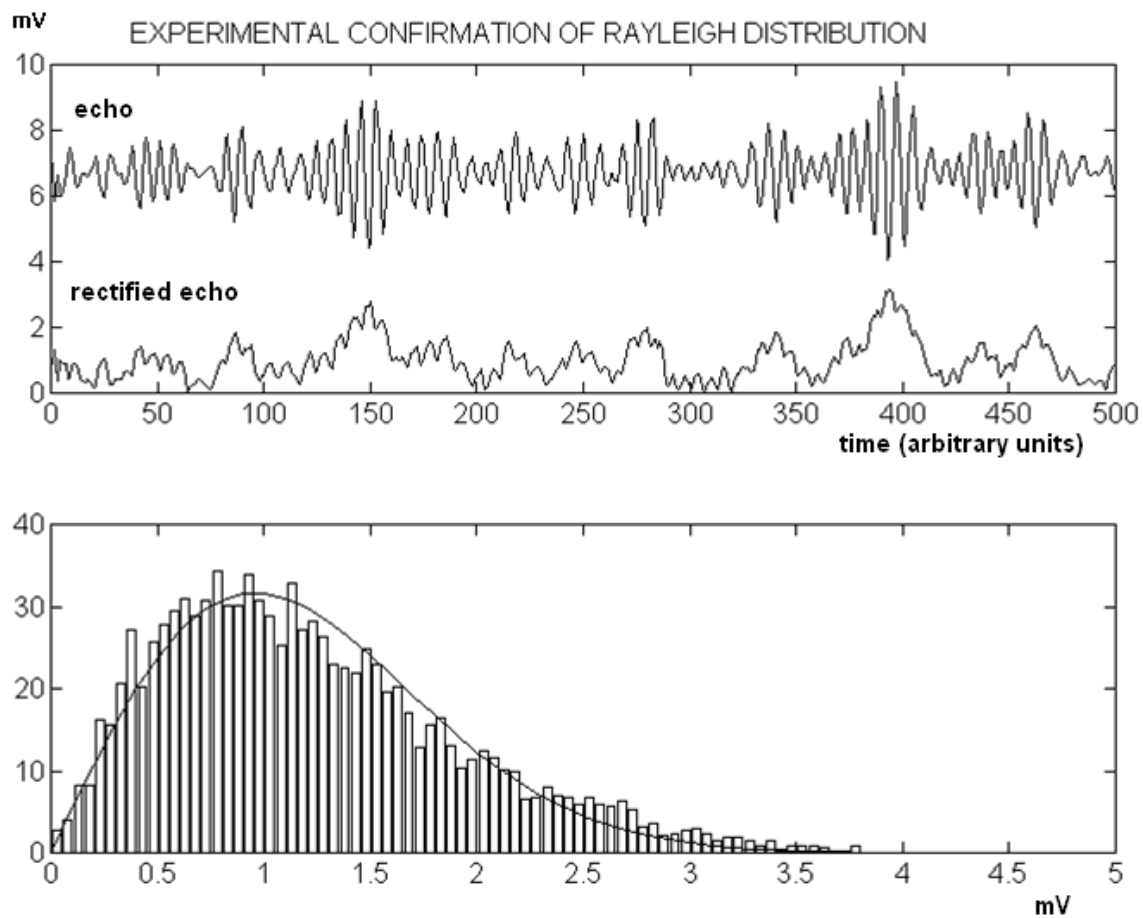
C-images of voids show the results of mathematical modelling of a single cylindrical void. There are 16 crosscuts (C-mages) of void simulation as input (upper images). The calculated "phantom images" (bottom images) calculated by 3D-convolution show the void shape distortions caused by speckle. In real phantom images it cannot be expected that there will be smaller distortions of voids, due to the structure of the foam. Variation of VDR will also occur with equal void sizes.

**Figure A.4 – C-images of voids**

### **A.2.3 Rayleigh Distribution of foam**

The structure of the foam leads to random scattering of the ultrasound. Therefore a Rayleigh distribution of echo levels can be expected.

The lower figure of Figure A.5 shows the comparison between the distribution of amplitudes of the rectified echo signals from foam and a Rayleigh distribution. Both distributions are shown on a linear scale. The image signals of a diagnostic ultrasound system are usually displayed on a logarithmic or log-like compression scale. The Rayleigh distribution changes to a normal distribution with logarithmic compression.



Upper figure: Upper line: Echo-signal of an amplitude scan.

Lower line: Rectified echo signal.

Lower figure: Histogram of the rectified echo signal and fitted Rayleigh distribution.

**Figure A.5 – Experimental confirmation of Rayleigh distribution with attenuating TMM**

#### A.2.4 Speed of Sound

Temperature and salinity influence the speed of sound. The sensitivity of the phantom for these influences can be estimated from data for salt water (without the foam) shown in Figure A.6. In a formula it is:

$$c = 1449,2 + 4,6 T - 0,055 T^2 + 0,00029 T^3 - [1,34 - 0,010 T ( S-35 )] + 0,01 z \quad (\text{A.1})$$

where

$c$  = speed of sound in  $\text{m s}^{-1}$ ;

$T$  = temperature in  $^{\circ}\text{C}$ ;

$S$  = salinity in weight parts per thousand;

$z$  = depth in m.

Data were taken from [8, 9, 10].

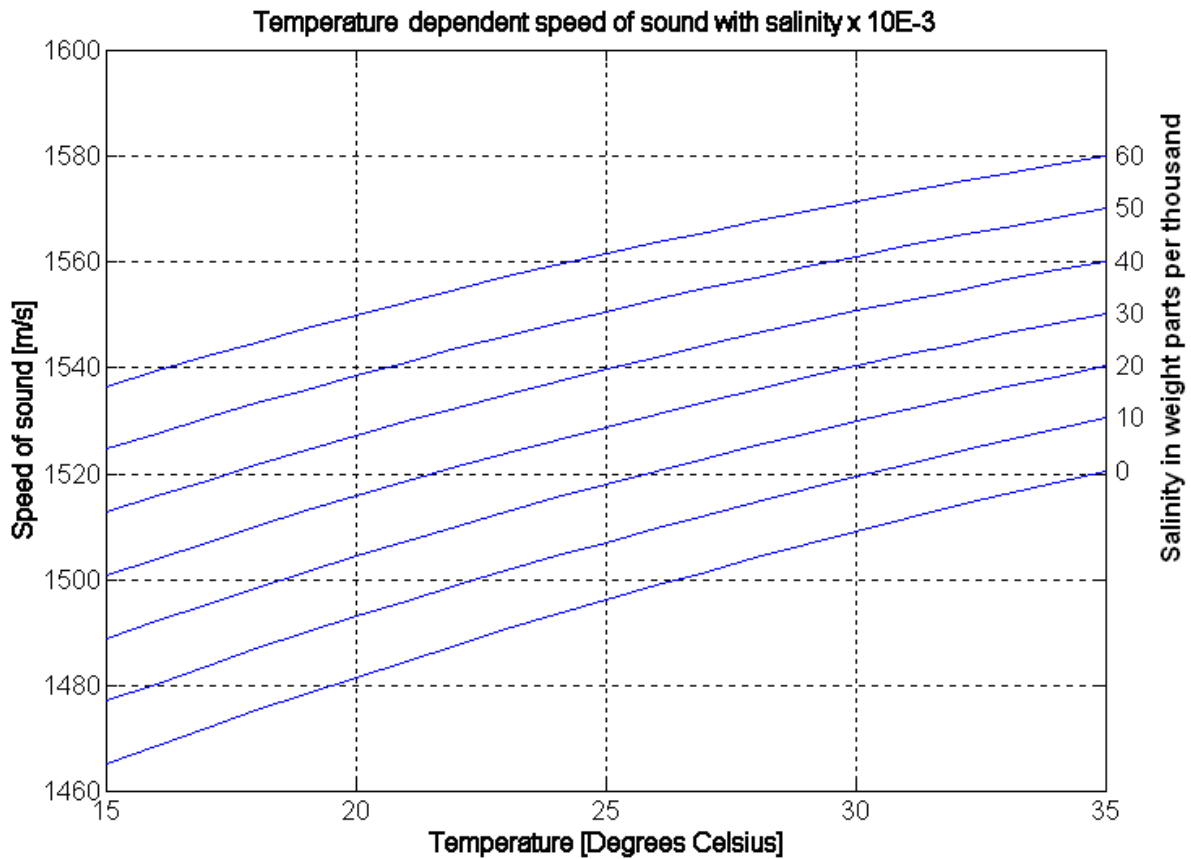


Figure A.6 – Speed of sound in saltwater

### A.3 Platform to adapt 3D-phantom to transducer for measurement



Figure A.7 – Phantom with motor drive and two types of adapters

The left side of Figure A.7 shows an exchangeable adapter for various types of transducers, e.g. linear, curved, phased array and sector transducers. The right side shows the adapter for endo-type transducers. The photo shows the adapter without a transrectal or transvaginal transducer.

At the top of the phantom the transducers are placed inside a sledge, which is either moved by hand or by a stepper motor drive. Two different adapters are available, one for general use, another for endo-type transducers (see Figure A.7). The movement of the sledge is

perpendicular to the B-scan plane of the transducer. Movement is possible both backwards and forwards. The transducer slides over the coupling surface of the phantom. In order to provide good acoustic contact between the transducer and the phantom a sufficient amount of acoustic coupling medium is administered between transducer and the window of the phantom. For curved transducers a water bath can be used as coupling.

The software in the PC causes the motor to scan regions of interest (ROI) underneath the acoustic window of the phantom. A sensor for probe position gives a feedback signal. This avoids alignment problems.

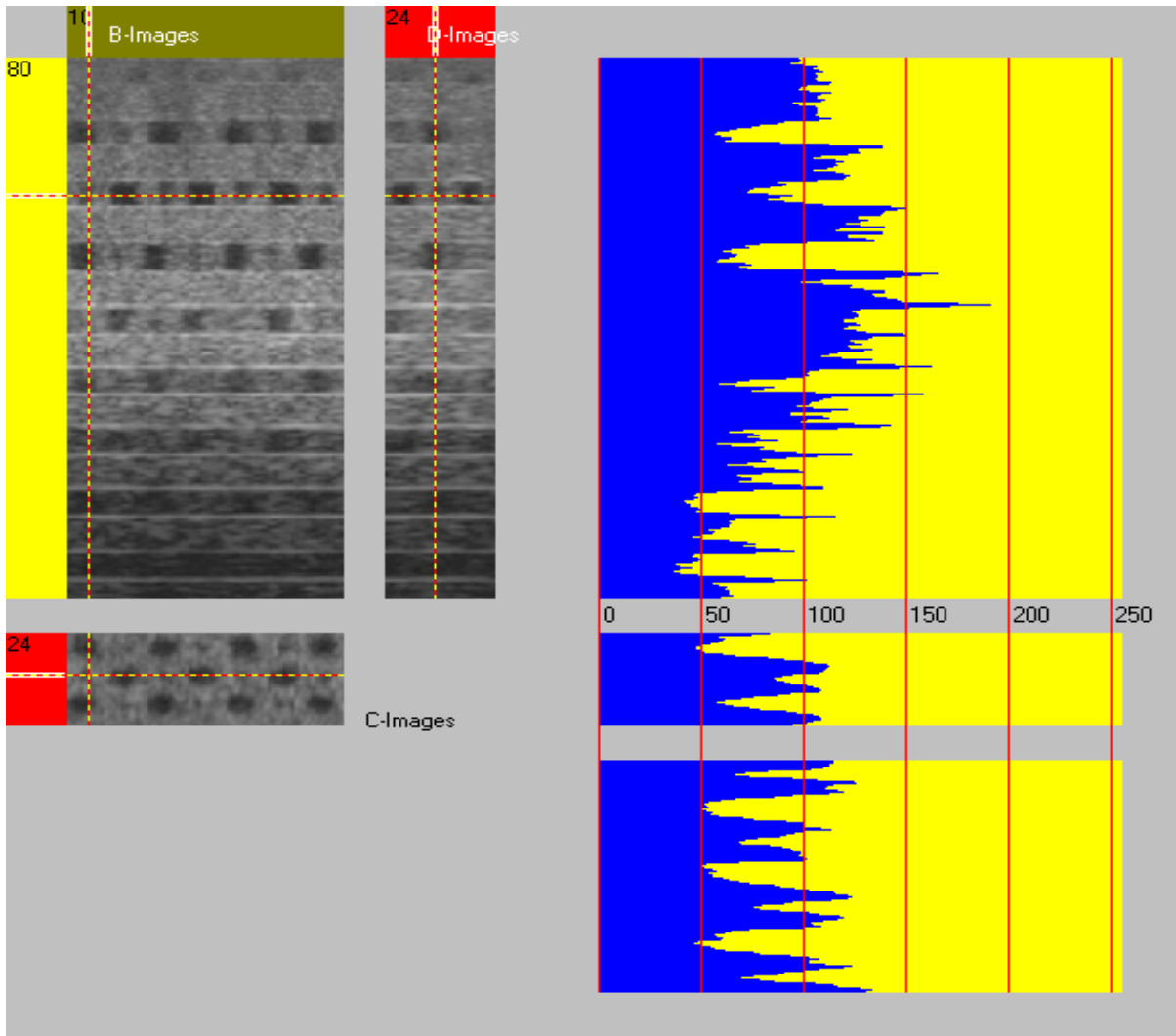
#### **A.4 Connection between ultrasound equipment and PC**

See Figure A.1. Images from the diagnostic ultrasound system are transferred in real time to the PC by applying a digitizer or converter, depending on the available signal output function of the diagnostic ultrasound system. A converter to use VGA or DVI output is available on the market. A frame grabber is recommended for diagnostic ultrasound systems with VHS or SVHS output.

#### **A.5 Measurement procedure**

The measurement is based on semi-automated operation. It comprises:

- (1) fixation of the related transducer on top of the phantom, ensuring proper coupling;
- (2) proper adjustment of the diagnostic ultrasound system (brightness, contrast, image size, dynamic range ( $\geq 60$  dB), pre-processing and post-processing controls);
- (3) connection of image output to the digitizer input of the PC;
- (4) adjustment of the digitizer and adjustment of the image recording window of the software;
- (5) start of the scanning (motorized or manual).



Left: B-, D-, C- image; voids are shown as dark areas. Right: Grey levels (horizontal scale) along three red lines in the image. From top to bottom on the right the lines represented are the intersections of planes BD, CD and BC.

**Figure A.8 – B-, D-, C- images and grey scale**

The software in the PC causes the motor drive to scan a ROI with constant speed. For visual checks, the phantom image in B-, C- and D-planes, together with the dynamic range in grey scale are displayed on the monitor of the PC (see Figure A.1 or Figure A.8). Also various presentations of VDR-values are possible (see below).

Evaluation of the data can be made off-line from the stored data. The ultrasound images are analyzed with dedicated software (see below). The first step in this analysis is to open a measurement series in a digitizer window on the screen and to identify manually the proper region of interest (ROI) inside the digitizer window. Thereafter automatic rendering of measured images can be started.

## A.6 Automated evaluation of the measurement results

The measurement process gives a stack of ultrasound images. These B-plane images are stored in a 3D matrix. From this matrix, both C-plane and D-plane images are constructed. The C-planes are parallel to the scanning surface; in C-planes the voids are displayed in a circular cross section.

The side-walls have an irregular contour due to the structure of the foam (see Figures A.3 and A.4). The D-planes are perpendicular to the B-planes and the C-planes. In the B-planes and the D-planes the voids are displayed as rectangles. (See Figure A.8 left side). The bottom and top of the voids often give strong signals due to coherent scattering, as can be seen in Figure A.8. The right side of Figure A.5 shows the grey level along three lines in the phantom, indicated by red lines on the images on the left side of Figure A.8. This type of display is useful to check that the grey level display is not in saturation and does not reach zero level. The large voids appear saturated if the dynamic range set at the diagnostic ultrasound system is below 60 dB.

## A.7 Calculation of VDR

To calculate values of VDR, the following procedure is adopted. First a region of interest (3D-ROI) is defined manually in the image. Usually this is a three-dimensional volume (as in Figure A.10) but for the explanation we use the data on a single line as in Figure A.5. In the 3D-ROI the automated discrimination between regions corresponding to voids and regions belonging to TMM is made with the following algorithm (see figure A.9).

Over the 3D-ROI the average signal level  $\mu_3$  is calculated. All points with a grey level  $g_i < \mu_3$  are classified as void, the remaining points are classified as TMM. High  $g_i$  values due to specular reflection at the bottom or top of voids are included in the TMM-values. For the points of TMM the mean value  $\mu_1$  and the standard deviation  $\sigma_1$  are calculated. For all voxels in the 3D-ROI,  $VDR_i$  is calculated from its grey level  $g_i$

$$VDR_i = (\mu_1 - g_i) / \sigma_1 \quad (\text{A.2})$$

The largest value of VDR occurring in a particular region (a line, a plane, a ROI or an image of a void) is used to characterize the signals in that region; of course, this corresponds to the point with the lowest grey level.

Thus  $VDR_V$  for a void is calculated from the lowest grey level  $g_V$  occurring inside the image of that void.

$$VDR_V = (\mu_1 - g_V) / \sigma_1 \quad (\text{A.3})$$

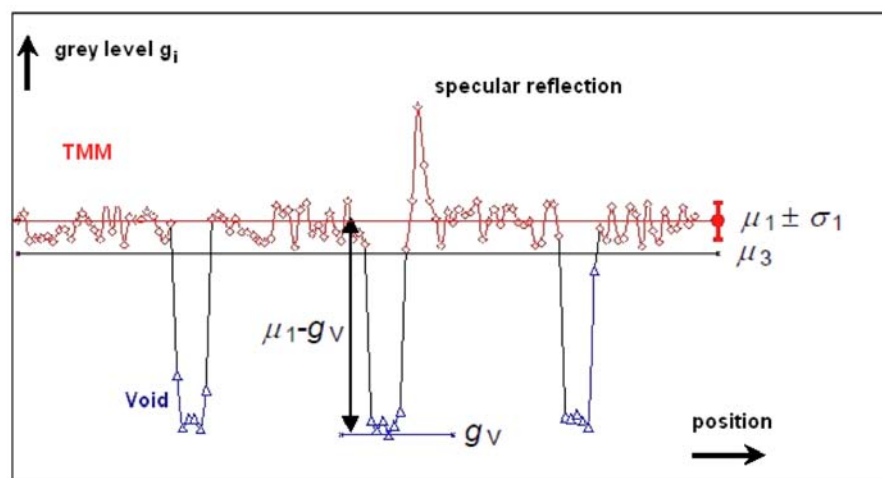


Figure A.9 – Illustration of the VDR calculation for a ROI consisting of a single line

Figure A.9 shows an illustration of the differentiation between points belonging to voids and points belonging to TMM, showing the terms used in Equations (A.2) and (A.3).

Displays with an inverted scale of grey levels were found to be useful, as voids are then white spots in black surroundings. These are easier to recognize than dark spots in a white background. The inverted grey scale is used in most of the following figures.

NOTE The definition of  $VDR_V$  assumes some speckle reduction has occurred in the ultrasound image processing, so that random zeros in the speckle do not make  $VDR_V$  an exceptionally noisy measure.

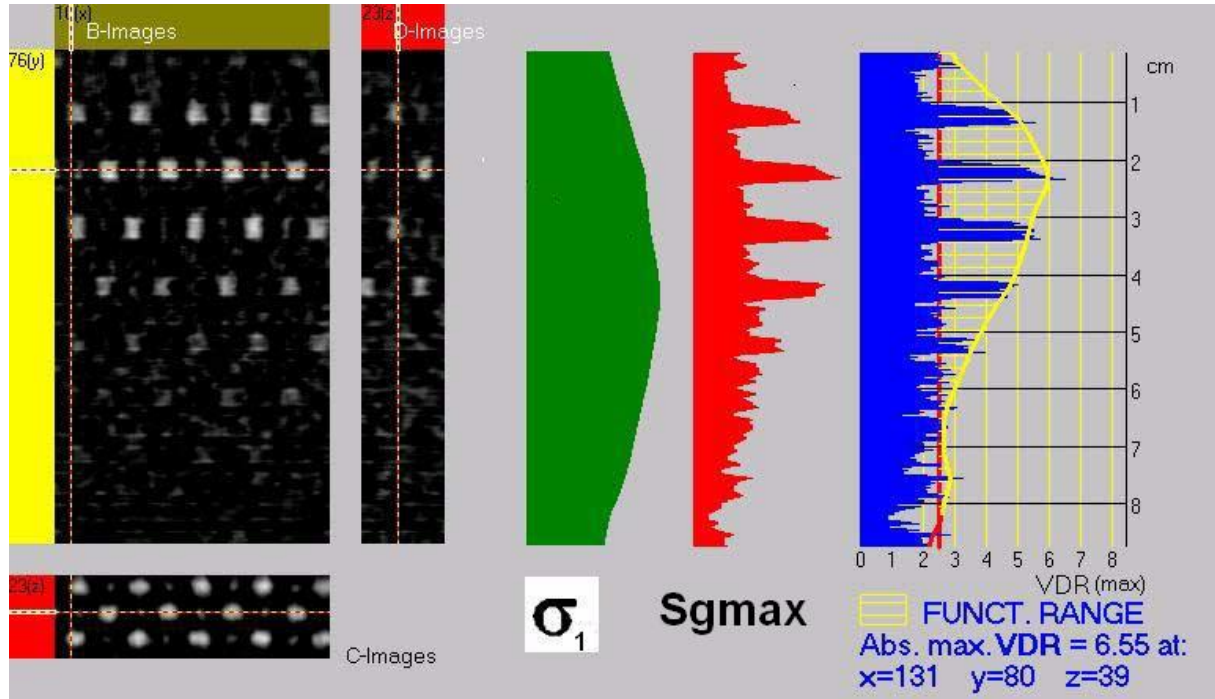


Figure A.10 – B-C-D planes

Figure A.10 shows:

Left: B-C-D-planes of the three-dimensional  $VDR_i$ -values that have been derived from the gray-scale information of the ultrasound images.

Right: For a stack of ROI's in consecutive C-planes, values of  $VDR(max)$  are shown as a function of depth. The position of the absolute maximum of  $VDR$  is given in x-y-z coordinates.

NOTE  $\sigma_1$  and  $S_{gmax}$  are shown as basic information without numerical scales, because the characteristics of receivers of ultrasound systems are different and it is not possible to compare "system A with system B". Comparable is only the voids' detectability within a single system.

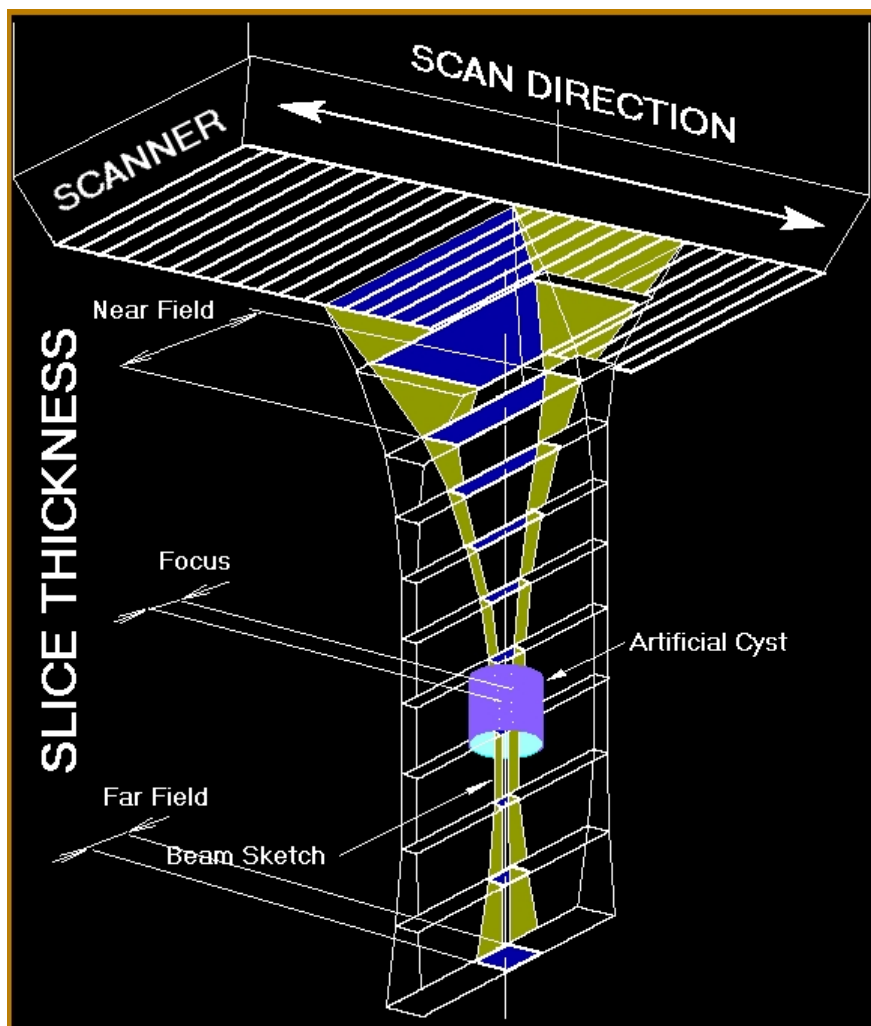
Figure A.10 shows for a particular case the grey scale images in three perpendicular B-, D-, and C-planes. On the right the three elements used in equation (A.2) are shown as a function of depth (in successive C-planes):  $\sigma_1$ ,  $S_{gmax} = \text{maximum value of } (\mu_1 - g_i)$ , and  $VDR(max)$ .

Notice that by using values in C-planes there is no need to align the ultrasound beam with the voids. By using the maximum value the best aligned beam with the void is selected for the calculation.

### A.8 Explaining geometry

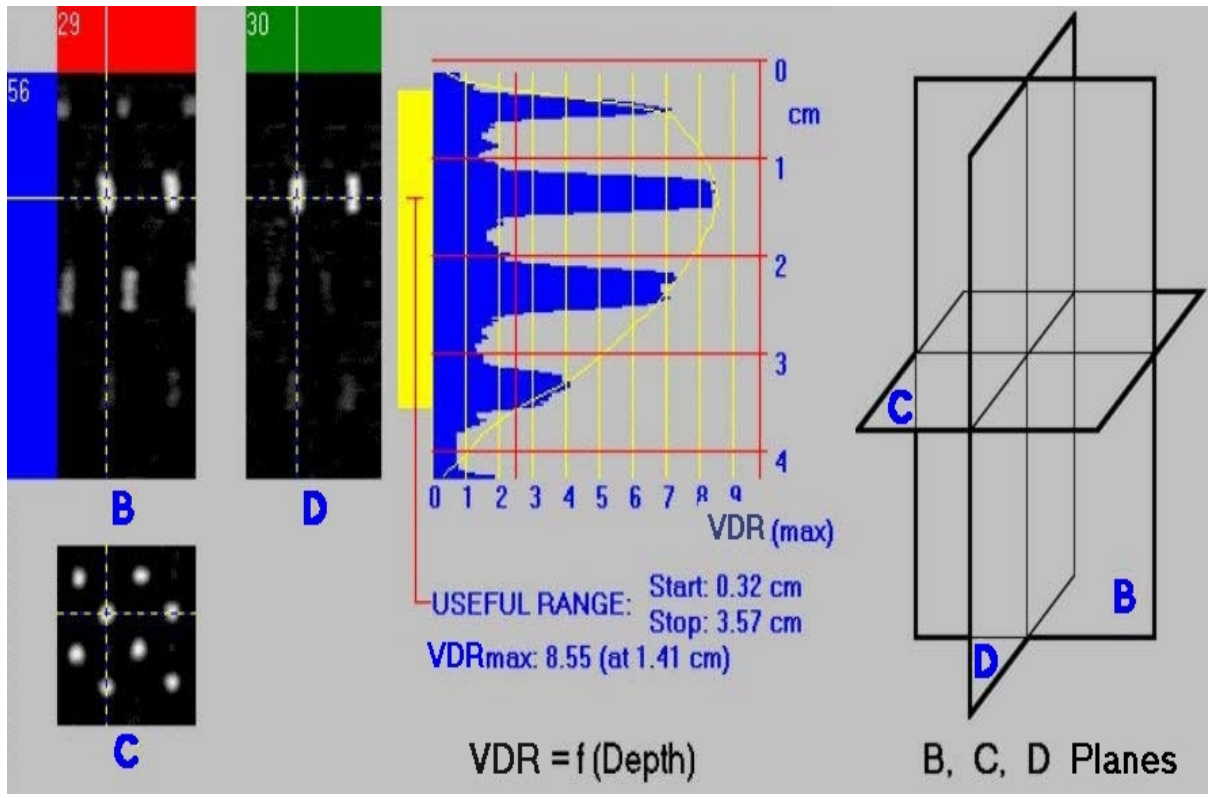
Figure A.11 shows the ultrasound beam passing through an artificial cyst within the phantom. Figure A.12 shows the relation between the geometry of the transducer (scanner) and the images in the B-, D-, and C-planes in Figure A.11. The ultrasound beam is shown at a particular moment during the scanning. Several piezo-crystals in the transducer cooperate to focus the beam in the B-plane (scan plane). Focussing in the elevational plane is obtained by

a passive lens structure. The diagnostic ultrasound system causes movement of the ultrasound beam in the B-plane, the motor drive displaces the transducer thus providing a movement in the D-plane. Different C-planes are obtained from the delay of the ultrasound echo.

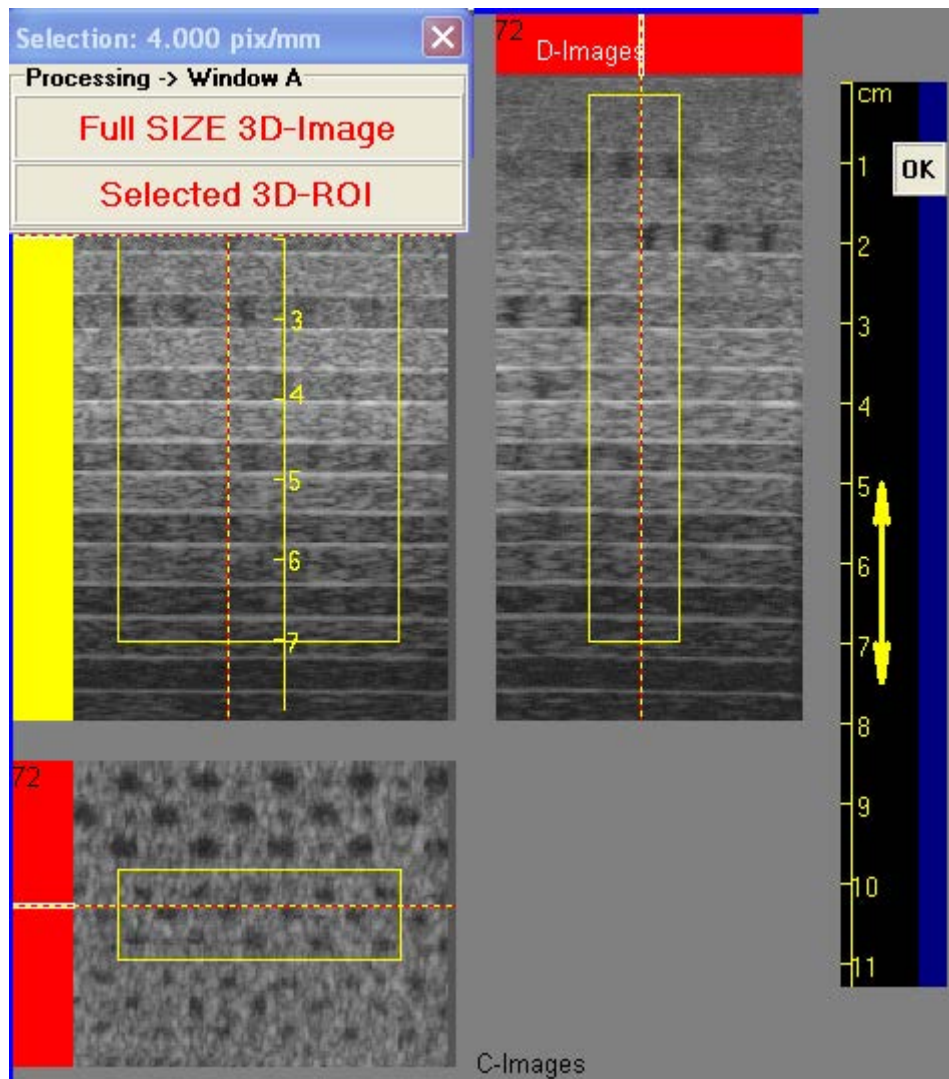


Principle of the ultrasound beam passing through the artificial cyst within the phantom.

**Figure A.11 – Principle of the ultrasound scanning array and beam**



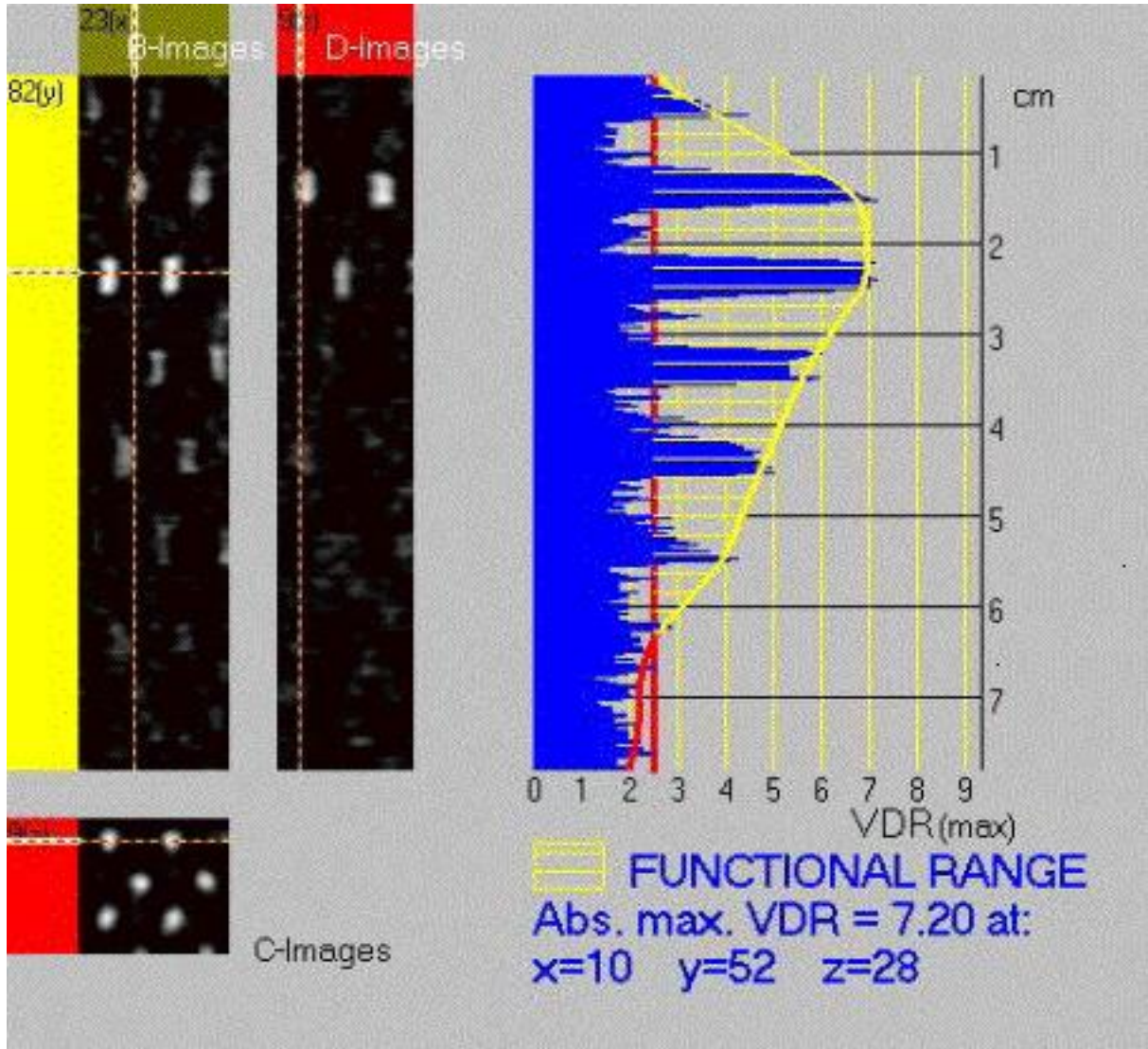
### A.9 Detectability of voids by measuring VDR



B-D-C planes and selected ROI, 3 mm and 1,5 mm, in C-images. Depth range shown in B and D-images.

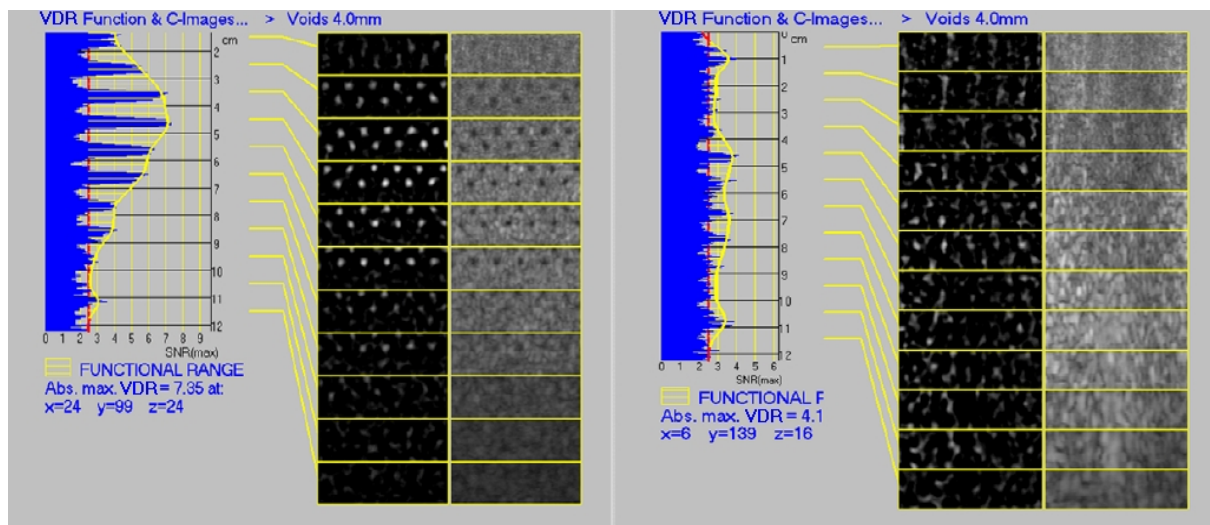
**Figure A.13 – 3D-Phantom images**

Volume acquisition of a phantom image is presented in Figure A.13 as B- C- and D-images in cross-sections “xyz”. The three visible lines in the B-D-C images show the intersection of the planes. In the C-image, three areas containing the different void sizes can be identified (as explained in 6.4: top: 2,5 and 1 mm, center: 3 and 1,5 mm, bottom: 4 and 2,5 mm). As shown in Figure A.13, ROIs are drawn manually and placed in the B-C images (yellow rectangles) to determine the desired voids to measure VDR. The decision which voids are included in the ROI is based on the frequency of the transducer (see 6.4). The black bar at the right side of Figure A.13 is necessary to calibrate slice thickness (2 slices = 10 mm) of the phantom image in regard to the scale factor of the ultrasound system. In Figure A.14 B-D-C images are displayed with grey scale inverted for better visualization; the functional range of VDR over depth is shown on the right.



Left: B-D-C images; Right: Functional range of VDR over depth. B-D-C images are displayed with grey scale inverted for better visualization.

**Figure A.14 – B-D-C images and VDR**



Curved arrays may be suitable for testing if their radii of curvature are large enough to provide a suitable image (left side above).

VDR-values near the limit of detectability of 4 mm voids.

**Figure A.15a) – Example: Curved Array, 40-mm radius, 3,5MHz with good VDR-values.**

**Figure A.15b) – Example: Curved Array, 40-mm radius, 3,5MHz with poor VDR-values**

### Figure A.15 – VDR-values

The following features should be noted in the figures above:

Figure A.15a): Blue diagram on the left side shows results for a curved array transducer, 40 mm radius, 3,5 MHz, with calculated VDR-values of detected voids in 4 mm and 2,5 mm diameter. The split images on the right side (C-images at the depths indicated by yellow lines) show resolvable voids. Grey levels are left inverted for better visualization. This transducer was three years in use.

Figure A.15b): Blue diagram on the left side shows calculated VDR-values of voids in 4 mm and 2,5 mm diameter and in the just-usable range between 4 cm and 5 cm depth. The split images on the right side (C-images at the depths indicated by yellow lines) show more artifactual signals than resolvable voids.

NOTE All curved arrays should be subjected to uniformity testing as described in Annex D before proceeding with other tests described in this technical specification.

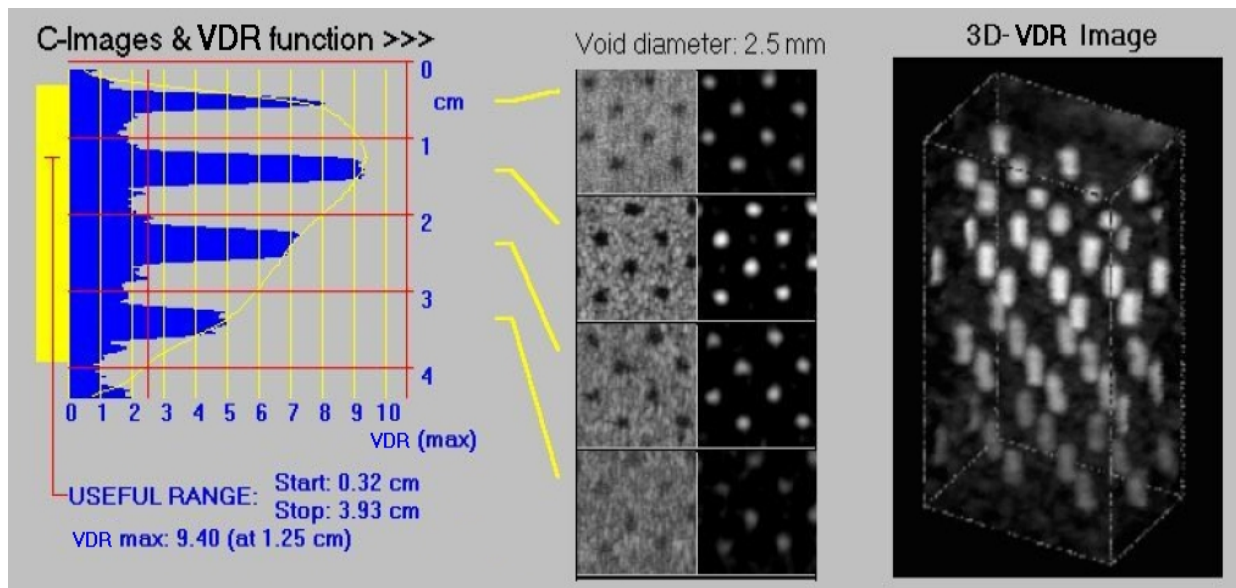


**Figure A.16 – Example: Linear array transducer 13 MHz**

Figure A.16 shows the usable range of a 13 MHz linear array transducer and clear display of detected voids of 2,5 mm and 1 mm diameter, together with display of visible voids in rendering. Rendering is part of the software and offers a more informative visual assessment of the VDR measurement.

## A.10 Interpretation of VDR Parameter

### A.10.1 Typical Features

This example shown in Figure A.17 is typical for a 3,5 MHz linear array transducer

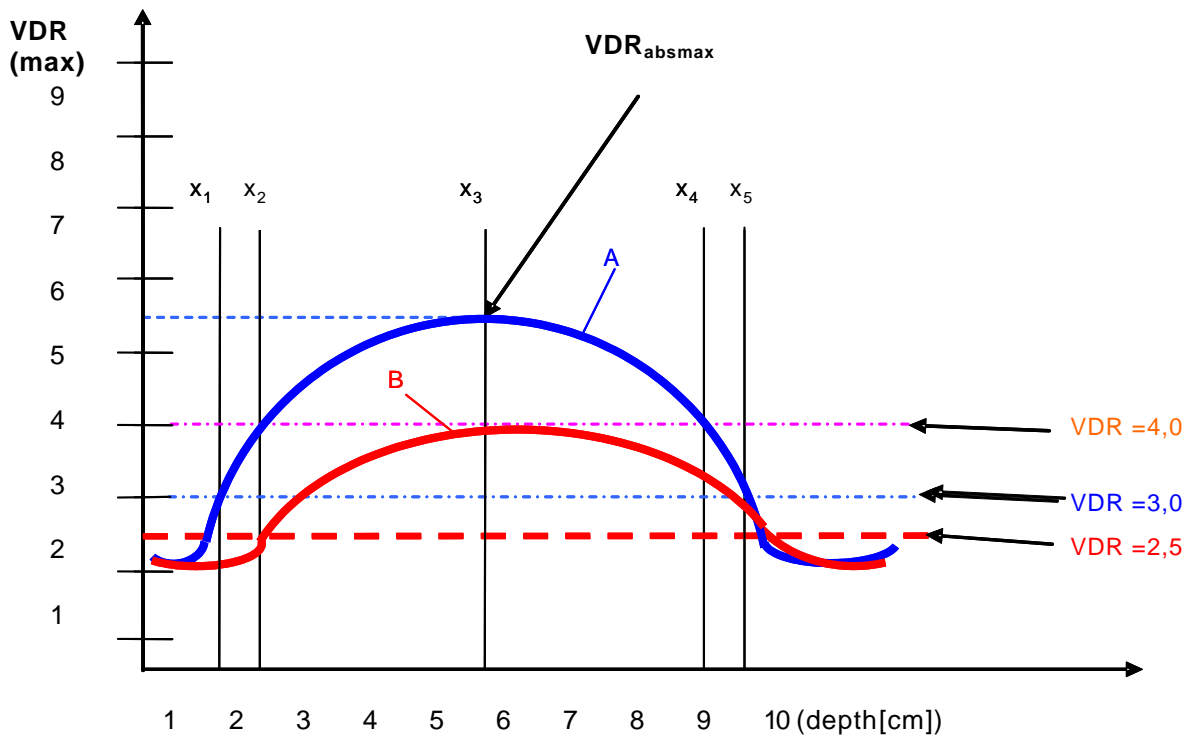


Figure A.17 – Interpretation of VDR parameter

The following features of Figure A.17 should be noted:

- **VDR(max) function A (blue curve):**

The curve represents the defined void detectability ratio.

It is a typical curve for good performance of a linear array transducer.

$VDR_{absmax}$  is variable and depends on the performance of the transducer, as well as being manufacturer- and type -dependent.

Depth of  $VDR_{absmax}$  is variable and depends on the selected scale of the diagnostic ultrasound system and specification of the related transducer.

The blue curve represents the  $VDR(max)$  function for an application depth range from  $x_2$  to  $x_4$ .

The depth to the position of  $VDR_{absmax}$  with the value  $x_3$  corresponds to the acoustic focal point of the overall system.

- **VDR(max) function B (red curve):**

This is a possible curve from the measurement of a similar linear array transducer with centre frequency of 3,5 MHz but with very low acoustical power ( $VDR_{absmax} \leq 4,0$ ). The transducer has reached the empirical border limit for applicable diagnostic use.

- **Threshold values of VDR:**

The empirical threshold for the measured detection of voids lies at  $VDR(max) = 2,5$  (red, dashed line). This line corresponds to the noise limit and no information from the image below this limit is achievable.

The empirical threshold for visual recognition of voids is represented by a void detectability ratio of approximately  $VDR(max) = 3,0$  (blue dot-dashed line).

$VDR(max)$ -values above this threshold encompass the maximum operating range of a diagnostic ultrasound system with a suitable transducer. This range is characterized by recognition of void sizes suitable for diagnosis.

The empirical threshold for good and safe visual recognition of voids is represented by a void detectability ratio of approximately  $VDR(max) = 4,0$  (pink dot-dashed line).  $VDR(max)$ -values above this threshold encompass the optimum operating range of a diagnostic ultrasound system with a suitable transducer. This range is characterized by 'good' recognition of the suitable void sizes.

### A.10.2 Saturation

As shown in Figure A.18, small and large voids produce similar wedges in the grey scale profile. The larger wedge is "cut" due to the shape of the local dynamic curve. For diagnostic ultrasound systems with large local dynamic range the saturation takes place only at low signal amplification. For comparison of the quality of identical diagnostic ultrasound systems and transducer types, the  $VDR_{absmax}$  cannot be taken alone as the measure of quality. The measure of quality depends on detectability of voids of defined sizes in regard to the related transducer frequency and VDR- value limits (see A.10.1)

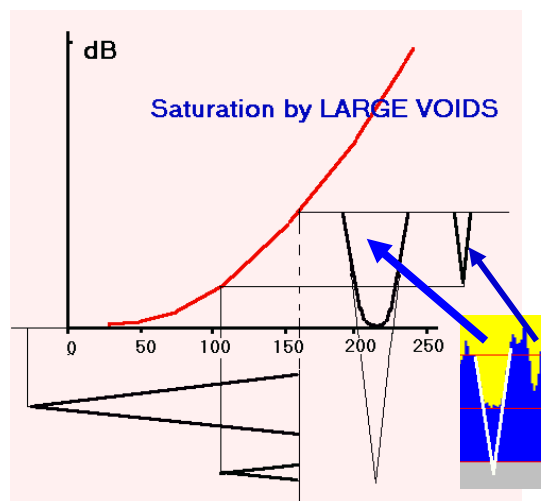


**Figure A.18 – Explanation of saturation (0-255 grey-scale range)**

The images in Figure A.19a) to A.19c) show the saturation effect visible on envelope shape with voids of 2,5, 3,0 and 4,0 mm for VDR distribution functions in dependence upon depth. The envelope shapes change because the  $VDR(max)$ - cannot reach the expected values. Saturation is soft and cannot be obviously seen. The following explanation will show how

saturation takes place in older types of diagnostic ultrasound systems or in current diagnostic ultrasound systems adjusted to low local dynamic range, below 50 dB.

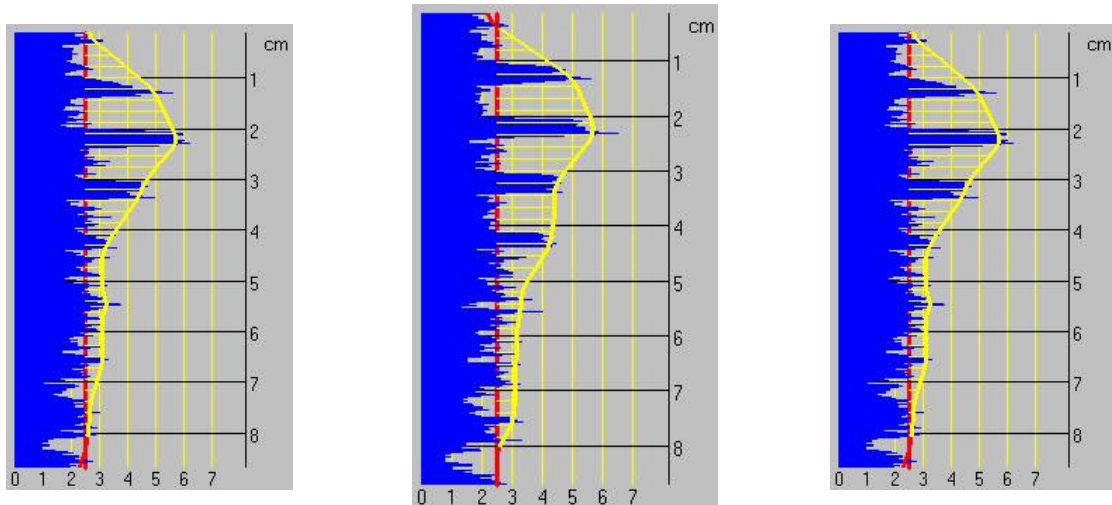


**Figure A.19a) – Voids  
2,5 mm**

**Figure A.19b) – Voids  
3,0 mm**

**Figure A.19c) – Voids  
4,0 mm**

**Figure A.19 – Saturation effect**

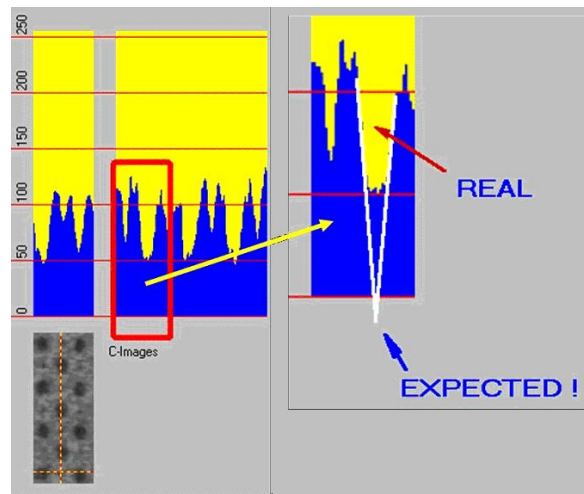


**Figure A.20 – Void spot analysis**

As shown in Figure A.20, small voids appear in grey-scale profile like sharp wedges. Large voids are however “cut” and appear not in the expected full size. The reason can be:

- saturation because of limited dynamic range;
- side-lobe- and grating lobe artifactual signals that “fill” the void;
- saturation and side-lobe artificial echoes taking place simultaneously.

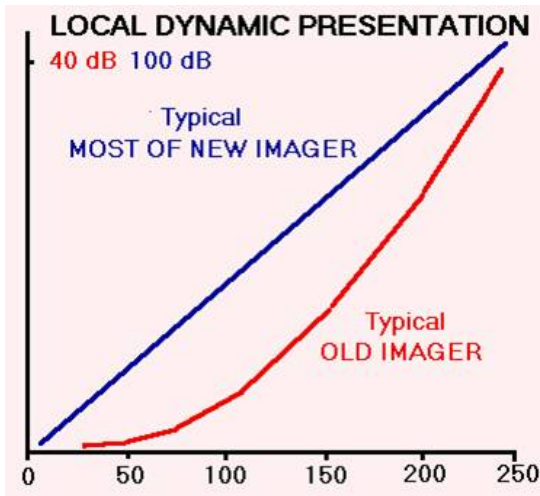


Figure A.21a) – Local dynamic curve

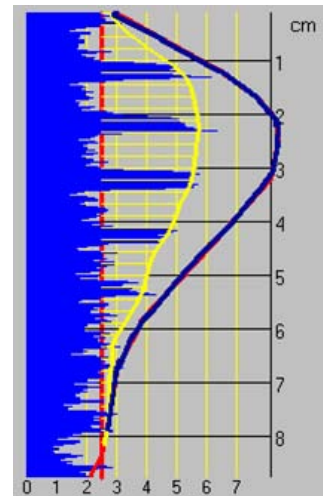


Figure A.21b) – Expected envelope of VDR

X-Axis: dB value; Y-Axis: Grey scale range

(blue curve)

### Figure 21 – Local dynamic range

As shown in Figure A.21a) most older diagnostic ultrasound systems have a limited local dynamic range between 40 dB to 50 dB and saturation takes place at “zero level”. Unfortunately many diagnostic ultrasound systems have lifted the “zero level” to a value of 30 dB to 50 dB in order to suppress the electronic noise.

Old and new diagnostic ultrasound systems differ in their local dynamic curves. The image in Figure A.21b) shows the expected VDR envelope (blue curve) as if the saturation would not take place. Modern diagnostic ultrasound systems have adjustable local dynamic range between 40 dB to 120 dB. Older diagnostic ultrasound systems have a limited dynamic range between 40 dB to 50 dB. Scale X in dB, Y in grey scale between 40 dB to 50 dB.

## **Annex B** (informative)

### **System description**

Test equipment required for tests of diagnostic ultrasound systems consists of:

- TMM 3D artificial-cyst phantom;
- platform with motor drive and adapter(s) to hold the different types of transducers during measurement as described in A.3;
- digitizer or frame grabber to convert real-time phantom image via available output from the diagnostic ultrasound system to Notebook or PC (VHS, S-VHS, VGA, DVI 2USB);
- software to install digitizer or frame-grabber with related ICON;
- software for data acquisition, processing, documentation with related ICONS;
- software for auto-correlation measurement to determine axial, azimuthal and elevation resolution of a given transducer at any point of the attenuation slices within the related depth of range of the phantom image display. For schematic diagrams refer to Figures C.2a) to C.2b);
- Software for uniformity measurement to determine uniformity of the complete transducer element array of linear and curved transducers, loss of elements prior to VDR measurement.

## **Annex C** (informative)

### **Rationale**

#### **C.1 General**

Many methods for measuring quality parameters of diagnostic ultrasound systems have been developed, while mechanical diagnostic ultrasound systems with single piezoelectric transducer elements were dominant and in the pre-digitizing era. With the introduction of multi-element transducers (linear, curved, phased, matrix arrays) the situation essentially changed.

With single-element transducers, the term “side lobes”, was almost unknown and seldom used. A small piezo-ceramic disk produces side lobes at the edge of the disk. With the apodization technique (or reduction of sensitivity at edges of a transducer disk), the side lobes were very much suppressed.

Arrays have many more “edges”, which produce more side lobes. Since the beginning of array technology, the “grating lobes” are a known problem. With adequate geometry of arrays (pitch) and acoustical matching, it is possible to reduce the grating lobes and other side lobes to a reasonable quantity.

Until now, the practice of visual assessment of diagnostic ultrasound system quality has not been abandoned. Many quality parameters can be measured automatically or semi-automatically. Not much interactive intervention is necessary for processing digitized image data.

If the primary goal is to measure parameters as precisely and as fast as possible, then the choice of tools has to be matched to these requirements. The measuring principles of today are based on a more adequate choice of measuring targets in test objects and phantoms with corresponding processing of ultrasound images.

Prior to performing VDR measurement a uniformity measurement is recommended (see Annex D). The uniformity measurement can be part of the software for “VDR” measurement and be accomplished without a phantom with an in vivo test e.g. on the forearm.

#### **C.2 Diagnostic ultrasound system quality parameters**

A description of the parameters can be found in the following literature:

- *AIUM Recommended Terminology* [12];
- *AIUM Methods For Measuring Performance Of Pulse-Echo Ultrasound Imaging Equipment, Part II: Digital Methods, Stage 1* [2].

#### **C.3 Autocorrelation function**

Another use of the phantom is display of elevational, azimuthal, and axial autocorrelation functions.

The auto-correlation [14] over one of the three dimensions is defined as:

$$ACwEl(\Delta x) = \sum_{x=0}^{X-1} \sum_{y=0}^{Y-1} \sum_{z=0}^{Z-1} f(x, y, z) f(x + \Delta x, y, z) \quad (C.1)$$

The auto-correlation function is a practicable resource to determine the elevational dimension independent of VDR measurement. Similar correlations are defined for the azimuthal (ACwAz) and axial (ACwAx) directions using the TMM 3D-phantom. Figure C.1 shows as an example a measurement of a 5,0 MHz linear transducer for all three directions at a depth of 4,57 cm.

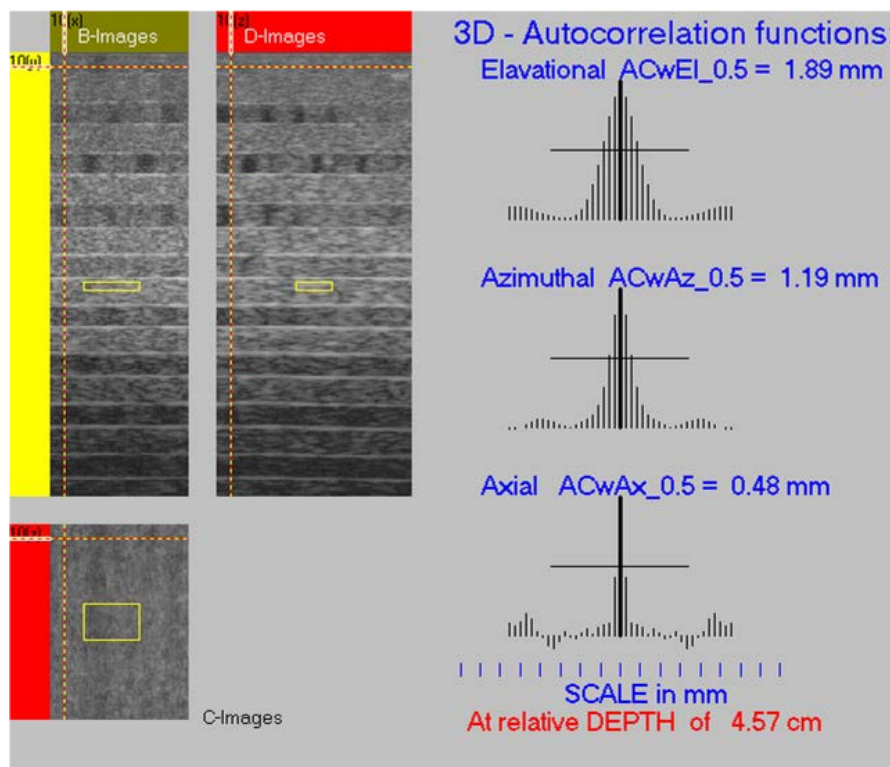


**Figure C.1 – Autocorrelation function**

Autocorrelation function is part of the software and applicable to determining axial, azimuthal and elevational resolution, independent of VDR measurement and post-processing. The autocorrelation uses the speckle information of the back-reflected US-signal. Any post processing that changes the speckle characteristics will reduce or destroy the information derived by this procedure. The procedure is as follows.

Select a 3D-phantom image and place an ROI as shown in an attenuation slice of the B-plane image; corresponding images are automatically displayed in the C- and D-plane. The ROI can be placed at any depth depending on scale depth. The autocorrelation function results will be displayed in graphical form together with respective values.

NOTE As the entire necessary information about images is acquired by the software, the use of this correlation method [14] may give additional information on the transducer properties. A detailed assessment of the interpretation of the correlation results is outside the scope of this document.

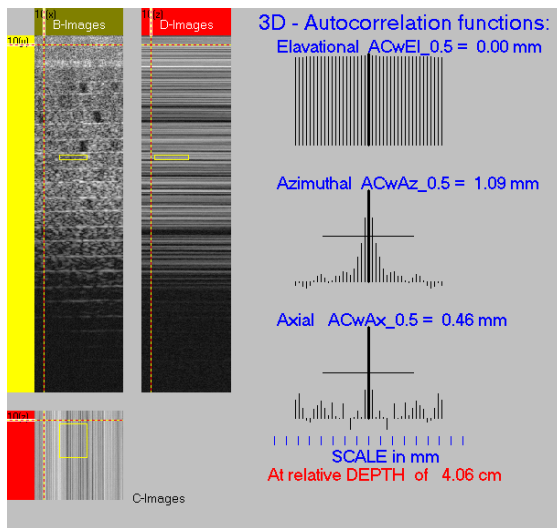


Figure C.2a) – Autocorrelation function at 4,06 cm depth

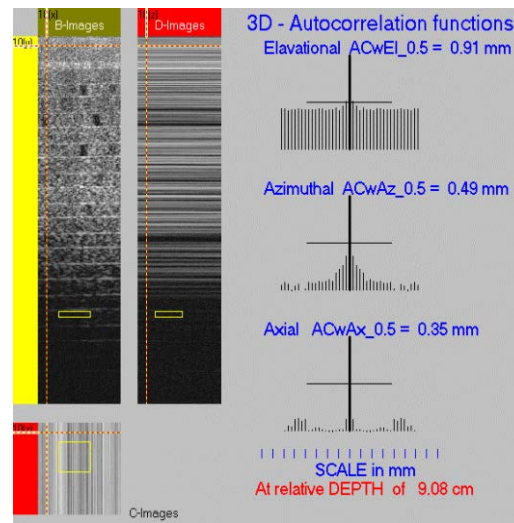


Figure C.2b) – Autocorrelation function at 9,08 cm depth

Figure C.2 – Autocorrelation function – dependence on depth

By setting the ROI (Figure C.2a) to the focal range the elevational autocorrelation function is near ~1 and electronic noise is negligible.

By setting the ROI (Figure C.2b) to the far field the elevational autocorrelation function will change. If the value of ~0,5 is registered, it can be taken as penetration depth

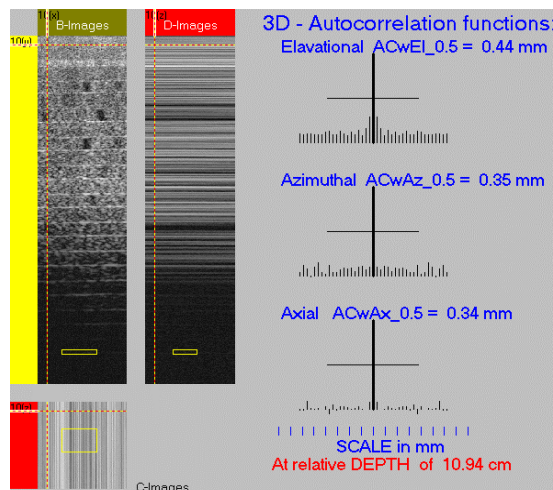


Figure C.3 – Autocorrelation function at 10,94 cm depth

Figures C.2a), C.2b) and C.3 illustrate the autocorrelation functions at various depths. As shown in these figures, the ultrasound image sequence is taken from the same position in space and without any changes in B-images, except electronic noise. The autocorrelation function in the D-direction is with a strong echo signal ~1, because electronic noise is negligible. In larger depth, the electronic noise begins to prevail and the echo signal slowly disappears. The autocorrelation value has a range from ~1 to zero (0). At the depth where echo signals totally disappear, the autocorrelation function is as expected, i.e. a 3D-delta function (Dirac function). In the range where autocorrelation is ~0,5 the contribution of echo signal is approximately equal to electronic noise. The mid-point of this range can be taken as depth of penetration.

## Annex D (informative)

### Uniformity measurement

#### D.1 General

A uniformity measurement method is a measuring method, providing information concerning the uniformity of electro-acoustical parameters of the separate elements in a transducer.

Most multi-element transducers operate in aperture mode, which means that each of the transmitted and received beams is generated by cooperation of more than one element (from ten to a few hundred). The transmitted ultrasound wave front is formed by interference of separate wave fronts generated by particular elements in the aperture. Different timing of excitation pulses to separate elements and changing numbers of elements in an aperture result in variability of a transmitted beam's focal-point position. Similar signal management is used for dynamic focussing during the receiving period. This means that every beam is created by an aperture consisting of more than one element. If one element fails, all the others remaining in the aperture mask the drop-out by their signals.

The influence of dead elements on the image quality depends on the ratio of the number dead to the total number in the aperture. A gap in an image created by a missing ultrasound line on the centre axis of the aperture appears only when all elements in the aperture are dead.

A "uniformity measurement" should be an obligatory part of the 3D-distribution of VDR measuring protocol, to demonstrate whether or not the uniformity criterion (mentioned in 7 in connection with curved arrays) is satisfied. The 3D-distribution of VDR-measurement does not have the capability to find a local defect of the transducer, due to its displaying only the maximum value of VDR for each C-plane. The local defect decreases VDR only when the ROI is limited exactly to the part of the scanned volume affected by the defect.

It is necessary to perform the "Uniformity measurement method" prior to measuring the 3D-distribution of VDR to detect a defective part of the transducer. When a defective part is detected, the 3D-distribution of VDR has to be measured over a scanned volume that must be limited to the volume affected by the defect only, to obtain the correct result. Otherwise the lower value of VDR is masked by the higher value of VDR from the "healthy" part of the transducer.

The test is easy to accomplish by scanning the forearm as shown in Figure D.1 to D.6 with linear or curved array type transducers. The primary condition for high quality ultrasound images may be defined as "properties equality" of all elements within the array or uniformity. The first step in the assessment of transducer quality is to find the variations of element sensitivity and loss of elements.

## D.2 Examples of linear and curved arrays



**Figure D.1a) – Uniformity test with related linear or curved array transducer**

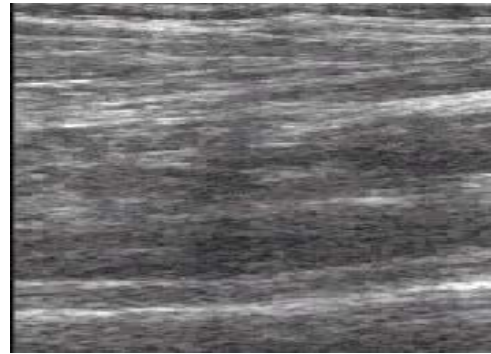
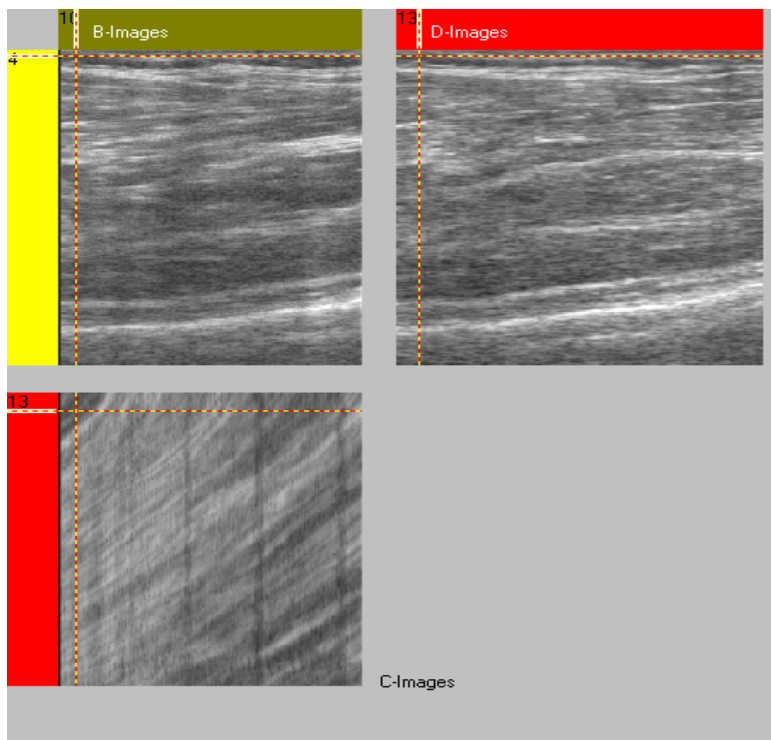


**Figure D.1b) – Fixed pattern in B-image**

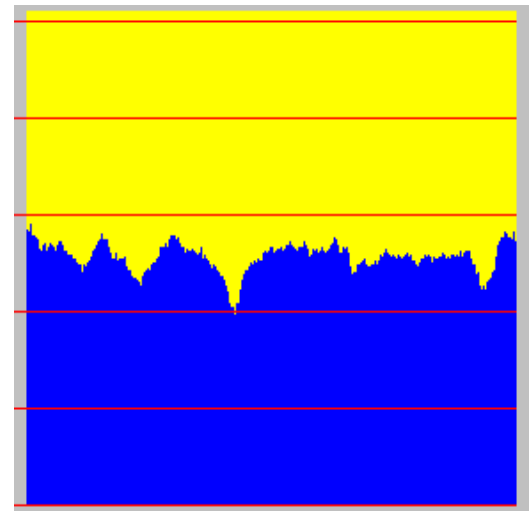
### **Figure D.1 – Uniformity test**

Figure D.1a) shows a uniformity test starting with scanning the forearm by moving the related transducer forth and back to take approximately 300 scans.

Figure D.1b) shows an unchanging, dark region within the image frame indicating a weak or disconnected element. In case of a visible fixed pattern an additional VDR-measurement is necessary.



**Figure D.2a) – B-D-C image and fixed pattern in C-image**



**Figure D.2b) – Grey scale display of full array**

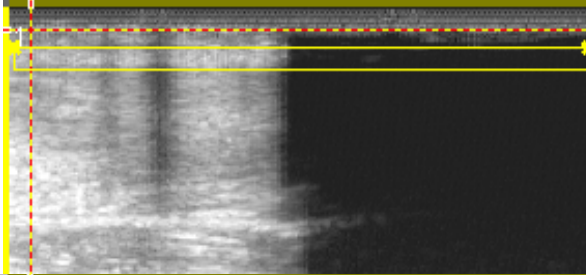
**Figure D.2 – Uniformity test – Additional features**

Figure D.2a) shows the fixed pattern that is more visible in the C-image. The fixed pattern as dark lines results from disconnected elements or reduced sensitivity of elements.

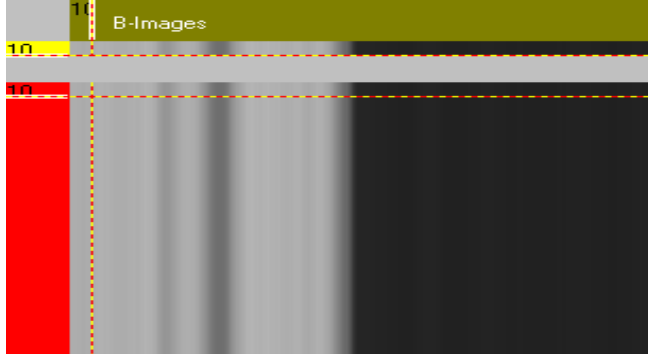
Figure D.2b): For analyses the C-image is converted in a grey-scale profile to show the full length of the array. The example shows disconnected elements. In case of evaluation of sensitivity variations of elements, it is necessary to use a reference.



Transducer covered with small strips of tape (5 layers) to simulate disconnected elements. The larger piece of tape simulates loss of sensitivity.



B-mode image with ROI marked by yellow lines over the length of the array. Fixed pattern simulating the disconnected elements.

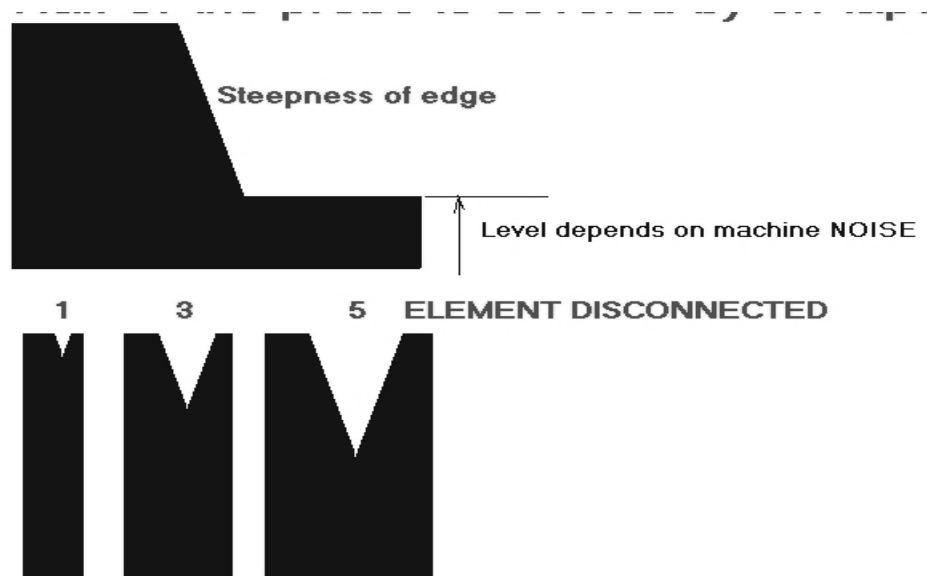


C-image shows the simulated disconnected elements more clearly.



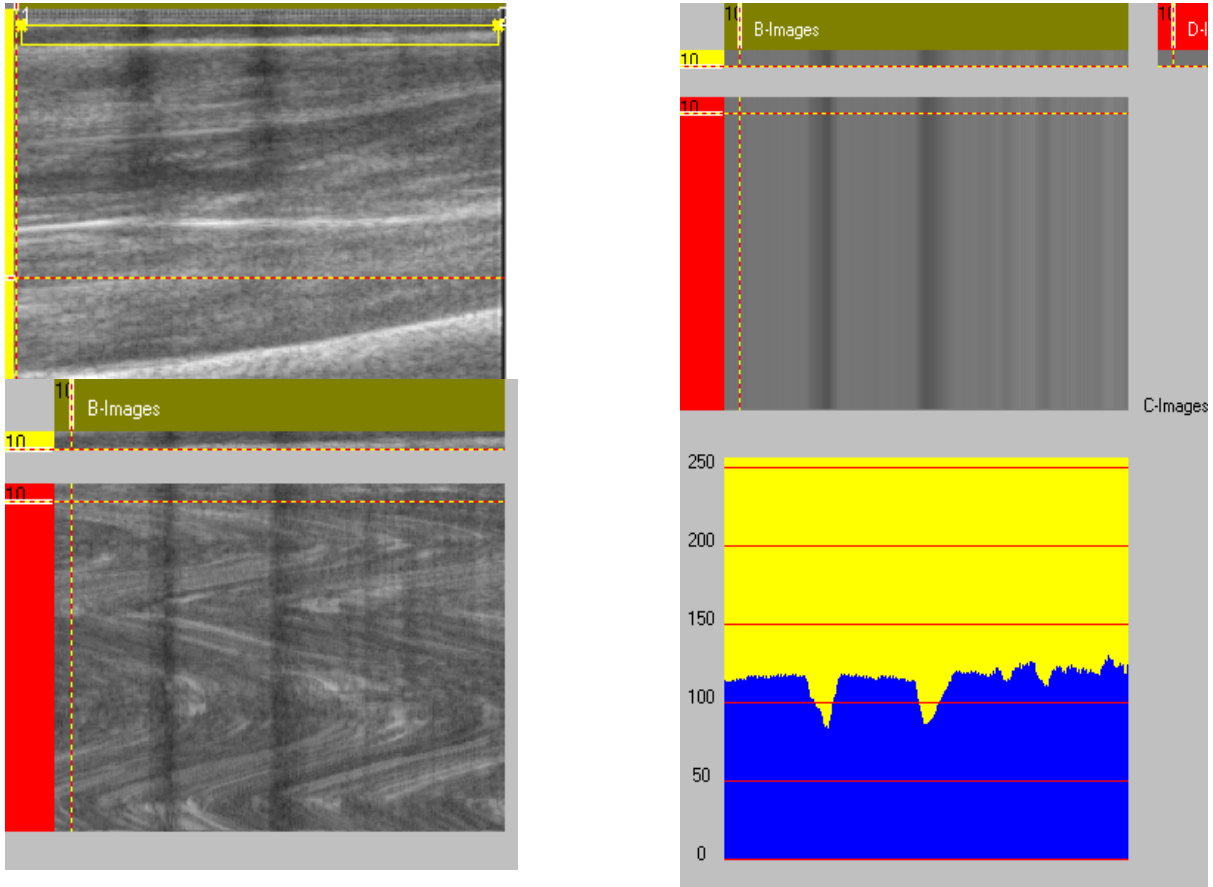
Grey scale profile showing the disconnected elements as smaller and larger wedges and on the right side loss of sensitivity of elements.

Figure D.3 – Linear transducer with reference tape



**Figure D.4 – Interpretation of simulated transducer failure when half of the probe is covered by five layers of 50-mm fabric tape**

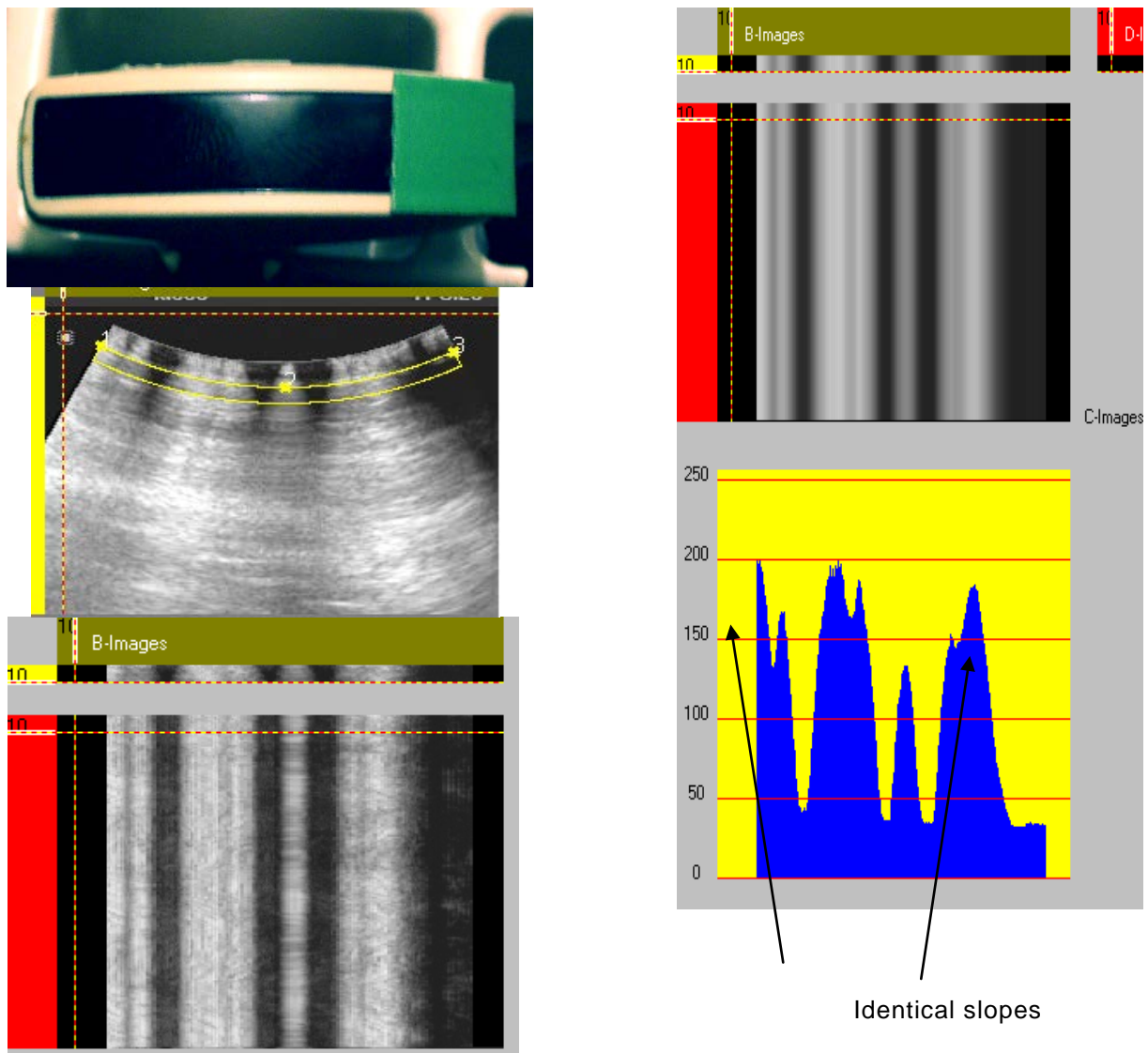
It can be expected that half of the transducer covered with high attenuation tape, e.g. five superimposed layers of fabric tape, e.g. TESA 4651, 50 mm, will produce the grey level as shown schematically. The tape does not abruptly cut the image of random scatter of the hand. Some steepness of the edge can be expected. Equal steepness can be expected by disconnected elements with typical wedge shape.



Left: Upper image with marked ROI over the length of array. Lower: fixed pattern in C-image.

Right: Upper B-image with fixed pattern, Lower: grey scale profile with wedges showing as loss of contributions from disconnected elements.

**Figure D.5 – Disconnected elements, example with linear transducer**



Left: Upper image: Curved array with tape reference, which shows in the near field reverberation in the lower image.

Middle: Curved array with marked ROI for near field rectification.

Lower: Black shadows showing disconnected elements. From left to right one or more elements near each other are disconnected.

Right: Compare upper image with indications of disconnected elements to lower image. The reverberation does not influence the reference slope visible for disconnected elements.

**Figure D.6 – Example with curved array transducer and reference tape**

## Bibliography

- [1] THIJSSSEN, JM, WEIJERS, G, DE KORTE, CL. Objective Performance Testing and Quality Assurance of Medical Ultrasound Equipment. *Ultrasound in Medicine & Biology*, 2007, 33, pp. 460-471
- [2] *Standard for Measuring Performance of Pulse-Echo Ultrasound Equipment*, American Institute of Ultrasound in Medicine, AIUM Technical Standards Committee, July 13, 1990, *Part II. Digital Methods, Stage 1*, AIUM 1995
- [3] PROCIAK, A. Cell structure and thermal conductivity of rigid polyurethane foams blown with cyclopentane in different molds. *PU-MAGAZINE*, March 2006, pp.104-106
- [4] ROWND, JJ, MADSEN, EL, ZAGZEBSKI, JA, FRANK, GR, DONG, F. Phantoms and Automated System for Testing the Resolution of Ultrasound Scanners. *Ultrasound in Medicine & Biology*, 1997, 23, pp.245-260
- [5] *AIUM Technical Standards Committee Quality Assurance Manual for Grey-Scale Ultrasound Scanners*, Stage 2, American Institute of Ultrasound in Medicine, 1995
- [6] SATRAPA, J, ZUNA, I, DOBLHOFF, G. *Differences of Ultrasound Propagation in Tissue and Tissue Mimicking Materials*, Acoustic Imaging, Vol.22, edited by P. Tortoli and L. Massotti, Plenum Press, New York,1996
- [7] SATRAPA, J, ZUNA, I, DOBLHOFF, G. *New Quantitative Support by Phantoms in Sonography*, Ultrasound World Congress 1995, Proceedings pp. 943 -946
- [8] CLAY, Clarence S, MEDWIN, Hermann. *Acoustical Oceanography*, John Wiley & Sons 1977
- [9] KINSLER, Lawrence E, FREY, Austin R, COPPENS, Allen B, SANDERS, James V. *Fundamentals of Acoustics*, John Wiley & Sons 1982
- [10] ETTER, Paul C. *Underwater Acoustics Modelling*, Elsevier 1991
- [11] *VDE-DGBMT Grundlegende Aspekte zur sicheren Anwendung von Ultraschall, Sicherheit und Qualitätssicherung von Ultraschallgeräten*, September 2004, pp.4-6
- [12] *AIUM Recommended Terminology*, American Institute of Ultrasound in Medicine, Third Edition, AIUM, 2008
- [13] *Digital Imaging and Communications in Medicine (DICOM) Part 1: Introduction and Overview*, Nat. Electrical Manufacturers Assoc., Rosslyn, VA, 2004, p. 21
- [14] DUNN, Patrick F. *Measurement and Data Analysis for Engineering and Science*, New York: McGraw–Hill, 2005
- [15] IEC 60761-1:2002, *Equipment for continuous monitoring of radioactivity in gaseous effluents – Part 1: General requirements*
- [16] IEC 61391-1, *Ultrasonics – Pulse-echo scanners – Part 1: Techniques for calibrating spatial measurement systems and measurement of system point-spread function response*
- [17] IEC 61391-2, *Ultrasonics – Pulse-echo scanners – Part 2: Measurement of maximum depth of penetration and local dynamic range*

- [18] IEC 62270:2004, *Hydroelectric power plant automation – Guide for computer-based control*
- [19] IEC 62453-1:2009, *Field device tool (FDT) interface specification – Part 1: Overview and guidance*

NOTE [5], [6], and [12] are referenced for information only.

---





INTERNATIONAL  
ELECTROTECHNICAL  
COMMISSION

3, rue de Varembé  
PO Box 131  
CH-1211 Geneva 20  
Switzerland

Tel: + 41 22 919 02 11  
Fax: + 41 22 919 03 00  
[info@iec.ch](mailto:info@iec.ch)  
[www.iec.ch](http://www.iec.ch)